A Szilikátipari Tudományos Egyesület lapja

építőanyag

Journal of Silicate Based and Composite Materials

A TARTALOMBÓL:

2013/2

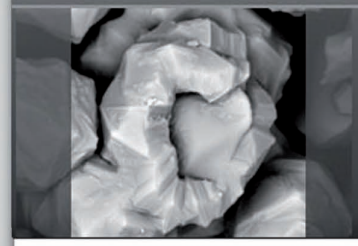

We are pleased to announce the organization of

ic-cmtp3

THE 3rd INTERNATIONAL CONFERENCE ON COMPETITIVE MATERIALS AND TECHNOLOGY PROCESSES

to be held at Hunguest Hotel Palota Lillafüred in Miskolc, Hungary, October 6-10, 2014.

The 2nd International Conference on Competitive Materials and Technology Processes was also held in this wonderful palace hotel in the exceptionally beautiful **Bükk Mountains** and together with coauthors have participated on it more than **550 scientists** from **36** countries of Asia, Europe, America and Africa.

The peer reviewed and accepted papers of **ic-cmtp3** conference will be published in periodicals of IOP Conference Series: Materials Science and Engineering (MSE) which are referred by Scopus, EI Compendex, Inspec, INIS, Chemical Abstracts, NASA Astrophysics Data System and many others. As organizers we hope you will submit your abstract and will attend on **ic-cmtp3** conference and we are looking forward to welcome you in **Miskolc, Hungary in October 6-10, 2014.**

The objectives

The event based more to academia than to industry and all papers will be peer reviewed before publication in **IOP Conference Series Materials Sciences and Engineering**, which is refereed by SCOPUS and many others. The international conference **ic-cmtp3** provides a platform among leading international scientists, researchers, engineers, students and PhD students for discussing recent achievements in research and development of material structures and properties of competitive materials like nanomaterials, ceramics, glasses, films and coatings, metals, alloys, biomaterials, composites, hetero-modulus and hybrid-materials, … etc.

Among the major fields of interest are materials with extreme physical, chemical, thermal, mechanical properties and dynamic strengths; including their crystalline and nano-structures, phase-transformations as well as methods of their technological processes, tests and measurements.

Promote new methods and results of scientific researches and multidisciplinary applications of material science and technological problems encountered in sectors like ceramics, glasses, metal alloys, thin films, aerospace, automotive and marine industry, electronics, energy, security, safety and construction materials, chemistry, medicine, cosmetics, biosciences, environmental sciences are of particular interests.

Sessions

Session 1: Advanced Materials for Bio- and Medical Applications
Session 2: Advanced Materials for Extreme Applications
Session 3: Advanced Nanomaterials with Predesigned Properties
Session 4: Biomaterial Derived Ceramics and Composites
Session 5: Glasses, Coatings and Related Materials
Session 6: Hetero-Modulus, Hetero-Viscous and Hybrid Materials
Session 7: Light-Weight Metals and Alloys
Session 8: Materials with Extreme Dynamic Strength for Safety and Security
Session 9: Membranes and Catalysts
Session 10: Minerals for Environmental and Medical Applications
Session 11: Nanomaterials for Environment and Health
Session 12: Novel Synthesis and Processing Technology
Session 13: Phase Diagram as a Tool of Materials Science
Session 14: Polymer Derived Ceramics
Session 15: Processing and Properties of Silicate Ceramics
Session 16: Refractory and Fireproof Materials
Session 17: Advanced Construction Materials

Important Dates

Please, be so kind and keep the following important dates of the 3rd International Conference on Competitive Materials and Technology Processes ic-cmtp3:

Sessions proposal deadline	December 20th, 2013
Abstract submission deadline:	February 28th, 2014
Notification of acceptance:	March 30th, 2014
Early registration deadline:	April 30th, 2014
Early registration fee payment deadline:	May 20th, 2014
Registration fee payment deadline:	August 10th, 2014

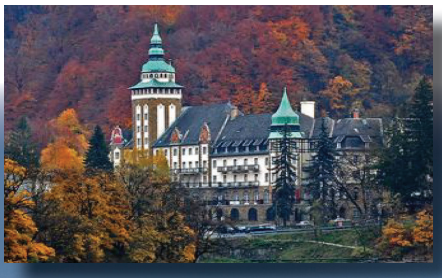

Further information can be obtained from Prof. Dr. László A. Gömze by e-mail femgomze@uni-miskolc.hu

építőanyag

Journal of Silicate Based and Composite Materials

2013/2

TARTALOM

CONTENT

A finomkerámia-, üveg-, cement-, mész-, beton-, tégla- és cserép-, kő- és kavics-, tűzállóanyag-, szigetelőanyag-iparágak szakmai lapja
Scientific journal of ceramics, glass, cement, concrete, clay products, stone and gravel, insulating and fireproof materials and composites

A folyóiratot referálja:
Cambridge Scientific Abstracts, ProQuest.
A szakmai rovatokban lektorált cikkek jelennek meg.
Kiadja a Szilikátipari Tudományos Egyesület
1034 Budapest, Bécsi út 122–124.
Telefon és fax: +36-1/201-9360
E-mail: epitoanyag@szte.org.hu
Felelős kiadó: ASZTALOS István SZTE elnök
Tördelő szerkesztő: NÉMETH Hajnalka

Címlapfotó/Cover photo by Eric Chenal

Egy szám ára: 1250 Ft
A lap az SZTE tagok számára ingyenes.

Belföldi terjesztés: SZTE
Külföldi terjesztés: Batthyany Kultur-Press Kft.

WWW.EPITOANYAG.ORG.HU

HU ISSN 00 13-970x INDEX: 2 52 50 ▪ 65 (2013) 33–60

65. évf. 2. szám

Crystallization paths in SiO_2-Al_2O_3-CaO system as a genotype of silicate materials

Vasily LUTSYK ▪ Institute of Physical Materials Science (Siberian Branch of Russian Academy of Sciences), Ulan-Ude, Russian Federation ▪ E-mail: vluts@ipms.bscnet.ru
Anna ZELENAYA ▪ Institute of Physical Materials Science (Siberian Branch of Russian Academy of Sciences), Ulan-Ude, Russian Federation ▪ E-mail: zel_ann@mail.ru
Érkezett: 2013. 08. 25. ▪ Received: 08. 25. 2013. ▪ http://dx.doi.org/10.14382/epitoanyag-jsbcm.2013.7

Abstract
The phases trajectories in the fields of primary crystallization of cristobalite (SiO_2^{cr}), tridymite (SiO_2^{tr}), mullite ($3Al_2O_3{\cdot}2SiO_2$) and in a field of liquid immiscibility are analyzed on a basis of computer model for T-x-y diagram of SiO_2-Al_2O_3-CaO system. The concentration fields with unique set of microconstituents and the fields without individual crystallization schemes and microconstituents are revealed.
Keywords: phase diagram, crystallisation path, SiO_2-Al_2O_3-CaO system, computer model

Vasily LUTSYK
Doct. Sci. (chemistry), Head of computer-aided materials design sector at the Institute of Physical Materials Science (Siberian Branch of the Russian Academy of Sciences). Research interests: functional ceramics, silicate systems for advanced technologies of building materials, pyrometallurgy, synthesis of refractory borides, silicides and intermetallics, metallic systems for lead-free solders.

Anna ZELENAYA
Cand. Sci. (phys.-math.), Senior Scientist at the Institute of Physical Materials Science (Siberian Branch of the Russian Academy of Sciences). Research interests: computer models of three-five phase diagram with different topology for microstructures design of heterogeneous materials, analysis of crystallization stages and identification the concentration fields with individual set of micro-constituents, simulation of phase diagram for ceramics, salt and metal systems.

1. Introduction

A phase diagram of system SiO_2-Al_2O_3-CaO (S-A-C) has wide applications and can be used in the cement industry to describe the properties of Portland and aluminous cements [1-3], and in studies of refractories and alkali-free glass [4]. To extend the capabilities of research and examine the processes of crystallization for S-A-C system allows its computer model [5-6]. Analysis of concentration fields obtained by the projection of phase regions onto Gibbs triangle allows to establish the boundaries of phase regions (located above the considered fields), the sequence of phase transformations and microstructural elements in crystallized initial melt at the equilibrium condition. Based on this technology, the research identifies fields with coinciding sets of crystallization scheme and microconstituents and the fields with individual characteristics.

2. T-x-y diagram model for SiO_2-Al_2O_3-CaO (S-A-C) system

The experimental data about the structure of S-A-C presented in the literature is usually confined to the surface of the primary crystallization (figure 1a) and triangles of coexistent phases [1-2, 7-9]. The spatial scheme of mono and invariant equilibria permits to restore the full construction of phase diagram. In the first stage a position of invariant planes are reproduced (figure 1b). Then the ruled surfaces of three-phase region borders are formed.

Let's consider the fragment of scheme adjoining to the component SiO_2 (figure 1c). The plane of four-phase regrouping of phases $L_U+SiO_2^{cr} \leftrightarrows R_5+SiO_2^{tr}$ has a degenerated structure $U\text{-}R5_U\text{-}S1_U(S2_U)$ ($S1=SiO_2^{cr}$ and $S2=SiO_2^{tr}$, ^{cr} – cristobalite, ^{tr} - tridymite), because the points $S1_U$ and $S2_U$ coincide together. Two ruled surfaces $S1_{e4}\text{-}e_4\text{-}U\text{-}S1_U$ and $R5_{e4}\text{-}e_4\text{-}U\text{-}R5_U$ bounding the phase region L+S1+R5 fit to the plane. The plane of ternary eutectic point E_4: $L^{E4} \rightarrow S2^{E4}+R5^{E4}+R12_2^{E4}$ ($S2_{E5}\text{-}R5_{E5}\text{-}R12_{E5}$) is arranged below. Three pairs of ruled surfaces ($S2_U\text{-}U\text{-}E_5\text{-}S2_{E5}$, $R5_U\text{-}U\text{-}E_5\text{-}R5_{E5}$; $S2_{E4}\text{-}E_4\text{-}[E_4,E_5]\text{-}S2_{E4,E5}$, $R12_{E4}\text{-}E_4\text{-}[E_4,E_5]\text{-}R12_{[E4,E5]}$; $R5_{Q8}\text{-}Q_8\text{-}E_5\text{-}R5_{E5}$, $R12_{Q8}\text{-}Q_8\text{-}E_5\text{-}R12_{E5}$) are bounded the phase regions L+S2+R5, L+S2+R12, L+R5+R12. The ruled surfaces $S2_{E4}\text{-}E_4\text{-}[E_4,E_5]\text{-}S2_{E4,E5}$, $R12_{E4}\text{-}E_4\text{-}[E_4,E_5]\text{-}R12_{[E4,E5]}$ are formed from the maximum point $[E_4,E_5]$ on monovariant curve E_4E_5. Three-phase region S2+R5+R12 situates below the simplex $S2_{E5}\text{-}R5_{E5}\text{-}R12_{E5}$.

Step-by-step restoring of phase regions boundaries permits to obtaine the complete model of phase diagram (figure 1d).

The projection of phase regions of system S-A-C divides the Gibbs triangle onto 117 two-dimensional, 163 one-dimensional and 45 zero-dimensional concentration fields. It is previously found that the projection of primary crystallization fields CaO, C_3S and C_3A are divided onto 52 concentration fields (19 two-, 21 one- and 12 zero-dimensional), among which 18 fields (12 one- and 6 zero-dimensional) haven't unique set of microconstituents [10].

Let's consider the fragment of phase diagram adjoining to component SiO_2 and carry out the analysis of concentration fields under the surfaces of primary crystallization cristobalite (SiO_2^{cr}), tridymite (SiO_2^{tr}), mullite (A_3S_2) and a cupola of melt immiscibility (i).

3. Structure of phase diagram adjacent to component SiO_2

There are 18 ruled surfaces, 4 horizontal planes at the temperatures of invariant points (E_4, E_5, Q_8, U), 4 vertical triangulation planes under the fields of primary crystallization SiO_2^{cr} (surface Q_{S1} with the contour $mknp_3Ue_4S$), SiO_2^{tr} (Q_{S2} – $e_3E_4[E4,E5]E_5Up_3$), A_3S_2 (Q_{A3S2} – $e_4UE_5Q_8e_5R5$) and the surface of immiscibility melt (i – k^0nkm) (figure 2, table 1). The following designations are used: e and p – binary eutectic and peritectic points, m and n – binary points of monotectic segment, E and Q – ternary eutectic and quasiperitectic points, U – point of the four-phase regrouping with participation of two polymorphous modifications SiO_2^{cr} and SiO_2^{tr}, $[E_4,E_5]$ – maximum point on the monovariant curve E_4E_5.

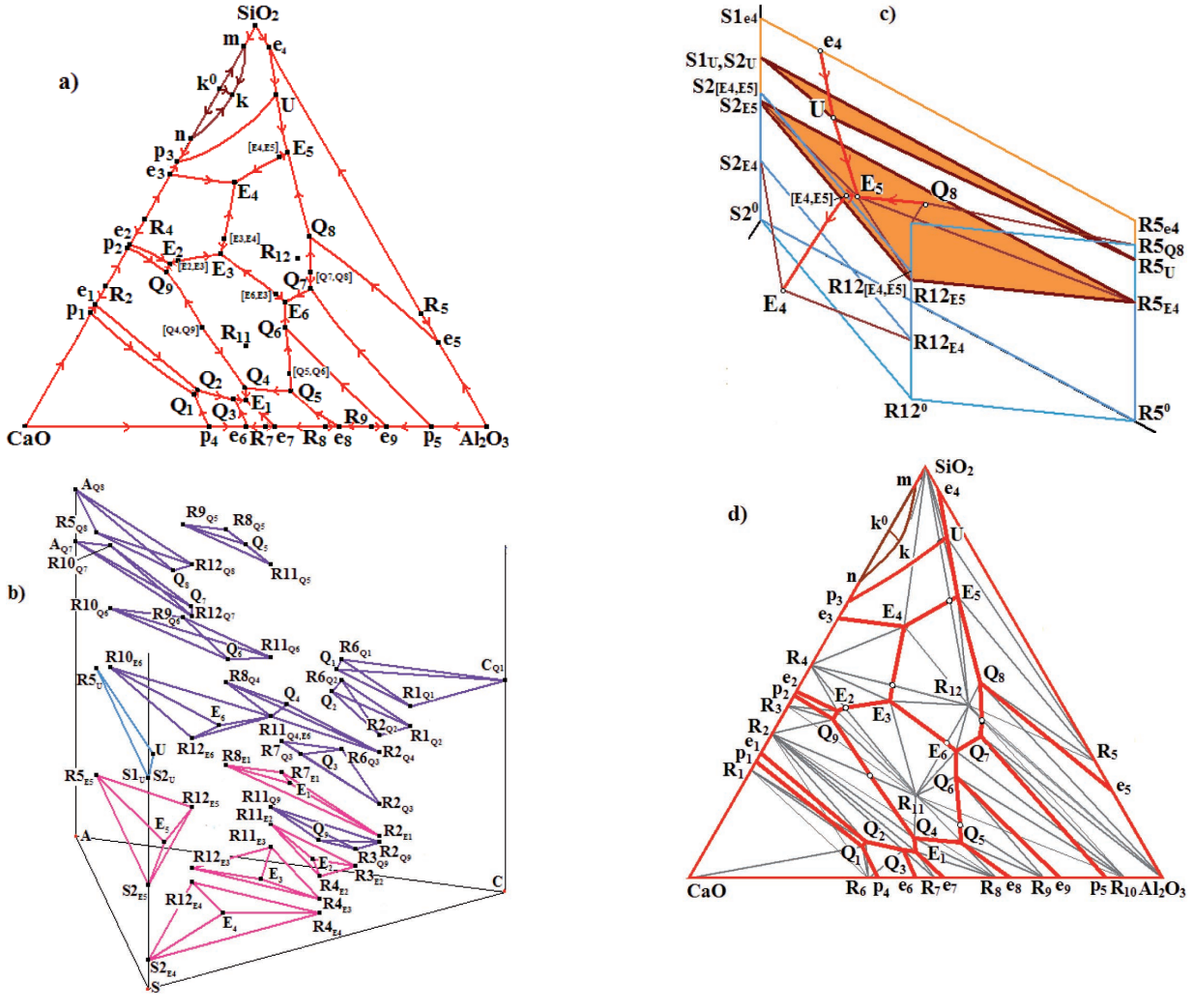

Fig. 1. XY projection of primary crystallization surfaces (a); 3D scheme of invariant planes arrangement (b) and three-phase regions of diagram fragment adjoining to the component S (c); XY projection of all phase regions (d) (R_1=C_3S, R_2=C_2S, R_3=C_3S_2, R_4=CS, R_5=A_3S_2, R_6=C_3A, R_7=$C_{12}A_7$, R_8=CA, R_9=CA_2, R_{10}=CA_6, R_{11}=C_2AS, R_{12}=CAS_2)

1. ábra Elsődleges kristályosodási felületek XY vetülete (a); invariáns síkok elhelyezkedésének 3D sémája (b); háromfázisú diagramszakaszok az S-fázishoz tartozóan (c); az összes fázisrész XY vetülete (d) (R_1=C_3S, R_2=C_2S, R_3=C_3S_2, R_4=CS, R_5=A_3S_2, R_6=C_3A, R_7=$C_{12}A_7$, R_8=CA, R_9=CA_2, R_{10}=CA_6, R_{11}=C_2AS, R_{12}=CAS_2)

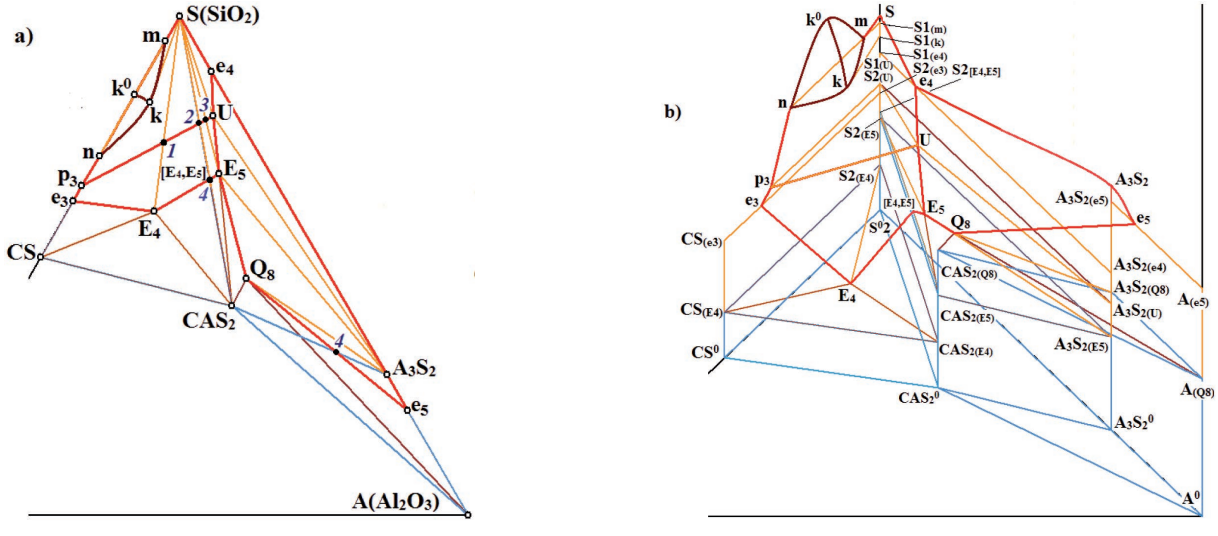

Fig. 2. XY projection (a) and 3D model (b) of fragment of system S-A-C phase diagram

2. ábra Az S-A-C fázisdiagram egy töredékének XY vetülete (a) és 3D modellje (b)

16 phase regions are located under the considered fields of primary crystallization: L_1+L_2, L+S1, L+S2, $L+A_3S_2$, $S+CAS_2$, $A+CAS_2$, $CS+CAS_2$, $A_3S_2+CAS_2$, L_1+L_2+S1, L+S1+S2, L+S2+CS, $L+S2+CAS_2$, $L+A_3S_2+CAS_2$, $S2+CS+CAS_2$, $A+A_3S_2+CAS_2$, $S+A_3S_2+CAS_2$ (table 2). The phase region L+S1+S2 is degenerated into line and the corresponding phase reaction proceeds at one temperature.

Symbol	Contour	Symbol	Contour
$Q^r_{e4\_A3S2}$	$A_3S_{2(e4)}$-e_4-U-$A_3S_{2(U)}$	$Q^r_{E4E5\_R12}$	$CAS_{2(E4)}$-E_4-[E_4,E_5]- $CAS_{2[E4,E5]}$
$Q^r_{E5U\_A3S2}$	$A_3S_{2(U)}$-U-E_5-$A_3S_{2(E5)}$	$Q^r_{E5E4\_R12}$	$CAS_{2(E5)}$-E_5-[E_4,E_5]- $CAS_{2[E4,E5]}$
$Q^r_{Q8E5\_A3S2}$	$A_3S_{2(Q8)}$-Q_8-E_5-$A_3S_{2(E5)}$	i^r	m-k-n
$Q^r_{e5\_A3S2}$	$A_3S_{2(e5)}$-e_5-Q_8-$A_3S_{2(Q8)}$	i^r_m	$S1_{(mn)}$-m-k-$S1_{(k)}$
$Q^r_{e4\_S}$	$S1_{(e4)}$-e_4-U-$S1_{(U)}$	i^r_n	$S1_{(mn)}$-n-k-$S1_{(k)}$
$Q^r_{E5U\_S}$	$S2_{(U)}$-U-E_5-$S2_{(E5)}$	H_{E4}	$S2_{(E4)}$-CS_{E4}-$CAS_{2(E4)}$
$Q^r_{e5\_A}$	$A_{(e5)}$-e_5-Q_8-$A_{(Q8)}$	H_{E5}	$S2_{E5}$-$A_3S_{2(E5)}$-$CAS_{2(E5)}$
$Q^r_{Q8E5\_CAS2}$	$CAS_{2(Q8)}$-Q_8-E_5- $CAS_{2(E5)}$	H_{Q8}	Q_8-$A_3S_{2(Q8)}$-A-$CAS_{2(Q8)}$
$Q^r_{e3\_S}$	$S2_{(e3)}$-e_3-E_4-$S2_{(E4)}$	H_U	U-$A_3S_{2(U)}$-$S1_{(U)}$,$S_{2(U)}$
$Q^r_{p3\_S}$	$S1_{(U)}$-p_3-U	$V_{S\text{-}CAS2}$	$S2_{[E4,E5]}$-$CAS_{2[E4,E5]}$-$CAS_2{}^0$-$S2^0$
$Q^r_{E4E5\_S}$	$S2_{(E4)}$-E_4-[E_4,E_5]-$S2_{[E4,E5]}$	$V_{A\text{-}CAS2}$	A_{Q8}-$CAS_{2(Q8)}$-$CAS_2{}^0$-$A_3S_2{}^0$
$Q^r_{E5E4\_S}$	$S2_{(E5)}$-E_5-[E_4,E_5]-$S2_{[E4,E5]}$	$V_{R5\text{-}CAS2}$	$A_3S_{2(Q8)}$-$CAS_{2(Q8)}$-$CAS_2{}^0$-$A_3S_2{}^0$
$Q^r_{e3\_CS}$	E_3-E_4-CS_{E4}-CS_{e3}	$V_{R4\text{-}CAS2}$	$CS_{(E4)}$-$CAS_{2(E4)}$-$CAS_2{}^0$-CS^0

Table 1. Contours of ruled surfaces (Qr, ir), horizontal (H) and vertical (V) planes
1. táblázat Az irányított felületek (Qr, ir) kontúrjai, vízszintes (H) és függőleges (V) síkok

4. Analysis of the concentration fields

At projection the surfaces Q_{S1}, Q_{S2}, Q_{A3S2} and i are divided onto 15 two-, 28 one- and 9 zero-dimensional concentration fields. Thirteen (2 two-, 8 one-and 3 zero-dimensional) fields coincide with neighbouring fields by the set of microconstituents.

The microconstituents of concentration fields corresponding to the regions of immiscibility melt (m-n-k, SiO_2-m-k, SiO_2-k, n-k, m-k, k) coincide with the of field p_3-1-SiO_2-k-n. Meanwhile the fields m-n-k, SiO_2-m-k and m-k differ from field p_3-1-SiO_2-k-n by intersected surfaces, phase regions and crystallization scheme (table 3). The phase region $L+S_1$ and phase region of immiscibility melt $L+S_1+S_2$ are located under the field SiO_2-m-k. At that the phase region $L+S_1$ is twice crossed for this field. So the field is characterized by two primary crystallization reactions $L^1 \rightarrow S_1{}^1$ between which the monotectic reaction $L_1{}^m \rightarrow L_2{}^m + S_1{}^m$ takes place. Field m-n-k arranges under the surface of immiscibility melt (i) and intersects the phase regions L_1+L_2 и $L_1+L_2+S_1$, where the phase reaction $L_1{}^1 \rightarrow L_2{}^1$ и $L_1{}^m \rightarrow L_2{}^m + S_1{}^m$ occur.

Since the process of melt immiscibility ends in the phase region $L_1+L_2+B_1$, then the reaction products $L_2{}^1$ and $L_2{}^m$ doesn't influence on the microconstituents forming. The crystals B_1 are not present in the microconstituents, because they are fully disappeared in the reactions $L^P,B_1 \rightarrow B_2{}^P$ and $L^U,S_1 \rightarrow S_2{}^U + A_3S_2{}^U$ and in the subsequent phase transformations there are only B_2 crystals. The reactions $L^P,S_1 \rightarrow S_2{}^P$ and $L^U,S_1 \rightarrow S_2{}^U + A_3S_2{}^U$ have degenerated form as the result of degeneration of phase regions $L+S_1+S_2$ in horizontal line and four-phase plane in the triangle U-$A_3S_{2(U)}$-$S1_{(U)}$,$S_{2(U)}$ [11].

The fields SiO_2-k, n-k and k coincide with field p_3-1-SiO_2-k-n by the list of phase reactions and the microconstituents.

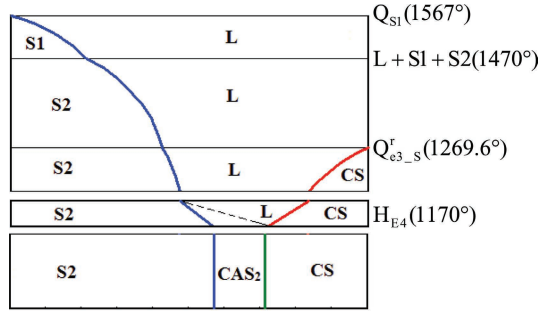

Fig. 3. Diagram of material balance for the concentration field p_3-1-SiO_2-k-n
3. ábra A p_3-1-SiO_2-k-n koncentráció mező anyag egyensúlyi diagramja

Let's consider the diagram of mass balances for composition given in the field p_3-1-SiO_2-k-n (figure 3). After the reaction of primary crystallization $L^1 \rightarrow S_1{}^1$ in the phase region L+S1 the composition falls into phase region $L+S_1+S_2$ (degenerated into line) where the crystals S_1 is fully disappeared as the result of reactions $L^P,S_1 \rightarrow S_2{}^P$ and $L^U,S_1 \rightarrow S_2{}^U + A_3S_2{}^U$. Then the composition moves into the phase region $L+S_2$ where the post-peritectical primary crystallization $L^{1P} \rightarrow S_2{}^{1P}$ takes place with the increasing of phase part S_2. In the phase region $L+S_2+CS$ the part of phase L is decreased and parts of phases S_2 and CS are increased: ($L^{eP} \rightarrow S_2{}^{ep(CS)} + CS^{ep(B2)}$). The phase L is fully disappeared as the result of reaction $L^{E4} \rightarrow S_2{}^{E4} + CS^{E4} + CAS_2{}^{E4}$

Symbol	Bounding surfaces	Symbol	Bounding surfaces
L_1+L_2	i, i^r	$L+A_3S_2+CAS_2$	$Q^r_{Q8E5\_A3S2}$, $Q^r_{Q8E5\_CAS2}$, H_{Q8}, H_{E5}, $V_{A3S2\text{-}CAS2}$
L+S1	Q_{S1}, i^r, $Q^r_{e4\_S}$, $Q^r_{p3\_S}$	$S2+CS+CAS_2$	$V_{S\text{-}CAS2}$, $V_{CS\text{-}CAS2}$, H_{E4}
L+S2	Q_{S2}, $Q^r_{e3\_S}$, $Q^r_{p3\_S}$, $Q^r_{E5U\_S}$, $Q^r_{E4E5\_S}$, $Q^r_{E5E4\_S}$	$A_3S_2+CAS_2+A$	H_{Q8}, $V_{A\text{-}CAS2}$, $V_{A3S2\text{-}CAS2}$
$L+A_3S_2$	Q_{A3S2}, $Q^r_{e4\_A3S2}$, $Q^r_{E5U\_A3S2}$, $Q^r_{Q8E5\_A3S2}$, $Q^r_{e5\_A3S2}$	$S2+A_3S_2+CAS_2$	$V_{A3S2\text{-}CAS2}$, $V_{S\text{-}CAS2}$, H_{E5}
L_1+L_2+S1	i^r, i^r_n, i^r_m	$S2+CAS_2$	$V_{S\text{-}CAS2}$
L+S1+S2	$Q^r_{p3\_S}$	$A+CAS_2$	$V_{A\text{-}CAS2}$
L+S2+CS	$Q^r_{e3\_CS}$, $Q^r_{e3\_S}$, H_{E4}	$A_3S_2+CAS_2$	$V_{A3S2\text{-}CAS2}$
$L+S2+CAS_2$	$Q^r_{E4E5\_S}$, $Q^r_{E5E4\_S}$, $Q^r_{E5E4\_CAS2}$, $Q^r_{E4E5\_CAS2}$, H_{E4}, H_{E5}, $V_{S\text{-}CAS2}$	$CS+CAS_2$	$V_{CS\text{-}CAS2}$

Table 2. Phase regions structure
2. táblázat Fázis területek szerkezete

Concentration fields	Intersected surfaces	Intersected phase regions	Crystallization scheme	Microconstituents
p_3-1-SiO_2-k-n	Q_{S1}, $Q^r_{p3\text{-}S}$, $Q^r_{e3\text{-}S}$, H_{E4}	$L+S_1$, $L+S_1+S_2$, $L+S_2$, $L+S_2+CS$, $B_2+CS+CAS_2$	$L^1\rightarrow S_1{}^1$, $L^p+S_1{}^1\rightarrow S_2{}^p$, $L^{1p}\rightarrow S_2{}^{1p}$, $L^{ep}\rightarrow S_2{}^{ep(CS)}+CS_4{}^{ep(B2)}$ $L^{E4}\rightarrow S_2{}^{E4}+CS_4{}^{E4}+CAS_2{}^{E4}$	$S_2{}^p$, $S_2{}^{1p}$, $S_2{}^{ep(CS)}$, $CS^{ep(B2)}$ $S_2{}^{E4}$, CS^{E4}, $CAS_2{}^{E4}$
SiO_2-m-k	Q_{S1}, i^r_m, i^r_n, $Q^r_{p3\text{-}S}$, $Q^r_{e3\text{-}S}$, H_{E4}	$L+S_1$, $L_1+L_2+S_1$, $L+S_1$, $L+S_1+S_2$, $L+S_2$, $L+S_2+CS$, $S_2+R_4+CAS_2$	$L^1\rightarrow S_1{}^1$, $L_1{}^m\rightarrow L_2{}^m+S_1{}^m$, $L^1\rightarrow S_1{}^1$ $L^p+S_1{}^{1,1p}\rightarrow S_2{}^p$, $L^{1p}\rightarrow S_2{}^{1p}$, $L^{ep}\rightarrow S_2{}^{ep(CS)}+CS^{ep(B2)}$ $L^{E4}\rightarrow S_2{}^{E4}+CS^{E4}+CAS_2{}^{E4}$	$S_2{}^p$, $S_2{}^{1p}$, $S_2{}^{ep(CS)}$, $CS^{ep(B2)}$ $S_2{}^{E4}$, CS^{E4}, $CAS_2{}^{E4}$
m-n-k	i, i^r, i^r_n, $Q^r_{p3\text{-}S}$, $Q^r_{e3\text{-}S}$, H_{E4}	L_1+L_2, $L_1+L_2+S_1$, $L+S_1$, $L+S_1+S_2$, $L+S_2$, $L+S_2+CS$, $S_2+CS+CAS_2$	$L_1{}^1\rightarrow L_2{}^1$, $L_1{}^m\rightarrow L_2{}^m+S_1{}^m$, $L^1\rightarrow S_1{}^1$, $L^p+S_1{}^1\rightarrow S_2{}^p$, $L^{1p}\rightarrow S_2{}^{1p}$, $L^{ep}\rightarrow S_2{}^{ep(CS)}+CS^{ep(B2)}$ $L^{E4}\rightarrow S_2{}^{E4}+CS^{E4}+CAS_2{}^{E4}$	$S_2{}^p$, $S_2{}^{1p}$, $S_2{}^{ep(CS)}$, $CS^{ep(B2)}$ $S_2{}^{E4}$, CS^{E4}, $CAS_2{}^{E4}$
SiO_2-k	Q_{S1}, $Q^r_{p3\text{-}S}$, $Q^r_{e3\text{-}S}$, H_{E4}	$L+S_1$, $L+S_1+S_2$, $L+S_2$, $L+S_2+CS$, $S_2+R_4+CAS_2$	$L^1\rightarrow S_1{}^1$, $L^p+S_1{}^1\rightarrow S_2{}^p$, $L^{1p}\rightarrow S_2{}^{1p}$, $L^{ep}\rightarrow S_2{}^{ep(CS)}+CS^{ep(B2)}$ $L^{E4}\rightarrow S_2{}^{E4}+CS^{E4}+CAS_2{}^{E4}$	$S_2{}^p$, $S_2{}^{1p}$, $S_2{}^{ep(CS)}$, $CS^{ep(B2)}$ $S_2{}^{E4}$, CS^{E4}, $CAS_2{}^{E4}$
n-k	Q_{S1}, $Q^r_{p3\text{-}S}$, $Q^r_{e3\text{-}S}$, H_{E4}	$L+S_1$, $L+S_1+S_2$, $L+S_2$, $L+S_2+CS$, $B_2+R_4+CAS_2$	$L^1\rightarrow S_1{}^1$, $L^p+S_1{}^1\rightarrow S_2{}^p$, $L^{1p}\rightarrow S_2{}^{1p}$, $L^{ep}\rightarrow S_2{}^{ep(CS)}+CS^{ep(B2)}$ $L^{E4}\rightarrow S_2{}^{E4}+CS^{E4}+CAS_2{}^{E4}$	$S_2{}^p$, $S_2{}^{1p}$, $S_2{}^{ep(CS)}$, $CS^{ep(B2)}$ $S_2{}^{E4}$, CS^{E4}, $CAS_2{}^{E4}$
m-k	Q_{S1}, i^r_m, i^r_n, $Q^r_{p3\text{-}B}$, $Q^r_{e3\text{-}B}$, H_{E4}	$L+S_1$, $L_1+L_2+S_1$, $L+S_1$, $L+S_1+S_2$, $L+S_2$, $L+S_2+CS$, $S_2+R_4+CAS_2$	$L^1\rightarrow S_1{}^1$, $L_1{}^m\rightarrow L_2{}^m+S_1{}^m$, $L^1{}_2\rightarrow S_1{}^1$, $L^p+S_1{}^{1,1p}\rightarrow S_2{}^p$, $L^{1p}\rightarrow S_2{}^{1p}$, $L^{ep}\rightarrow S_2{}^{ep(CS)}+CS^{ep(B2)}$ $L^{E4}\rightarrow S_2{}^{E4}+CS^{E4}+CAS_2{}^{E4}$	$S_2{}^p$, $S_2{}^{1p}$, $S_2{}^{ep(CS)}$, $CS^{ep(B2)}$ $S_2{}^{E4}$, CS^{E4}, $CAS_2{}^{E4}$

* [1] – primary crystallization $L^1\rightarrow I^1$; [e] – monovariant eutectic reaction $L^e\rightarrow I^e+J^e$; [p] – monovariant peritectic reaction $L^p+A^p\rightarrow R^p$; [m] – monovariant monotectic reaction $L_1{}^m\rightarrow L_2{}^m+R^m$; [E] – invariant eutectic crystallization $L^E\rightarrow B^E+C^E+R^E$; [Q] – invariant quasiperitectic regrouping of masses $L^Q+A^Q\rightarrow B^Q+R^Q$; [1p] – post-peritectic primary crystallization $L^{1p}\rightarrow R^{1p}$; [ep] – post-peritectic monovariant crystallization $L^{ep}\rightarrow R^{ep}+J^{ep}$ (J=B, C)

*Table 3. Crystallization scheme and microconstituents for surface of immiscibility i and the fragment of primary crystallization surface Q_{S1} of high-temperature modification SiO^r_2 (S1)**

3. táblázat Kristályosodási séma és mikro-összetevők az i oldhatatlansági felülethez és a Qs1 elsődleges kristályosodási felület töredéke a SiO^r_2 (S1) módosulására magas hőmérsékleten*

on the plane at the temperature of ternary eutectic points E_4. Below the plane the composition gets to the solid-phase region $S_2+CS+CAS_2$.

The concentration fields e_4-U and U coincide with fields SiO_2-U-e_4 и SiO_2-U by the microconstituents, but differ the crystallization scheme. Fields e_4-U and U haven't the reaction of primary crystallization $L^1\rightarrow B_1{}^1$. The concentration fields p_3-1 and 2 differ from fields e_3-E_4-1-p_3 and 2-4 by intersected surfaces. The fields E_5-3, A_3S_2-U и A_3S_2-Q_8 are identical with E_5-U-3, U-E_5- A_3S_2 and E_5-Q_8-A_3S_2 by the microconstituents and crystallization scheme correspondently.

5. Conclusion

Computer model of PD gives the possibility to analyze the crystallization stages for any composition and to find the concentration fields both with individual set of microstructure elements and the fields at which the crystallization scheme and microconstituents of phases assemblage coincide with those in the adjoining fields. It is used as an important tool to investigate multicomponent system, to correct its constitutional diagram, to design the miscrostructures of heterogeneous material, to decipher the genotype of heterogeneous material [12]. One more reason for the microstructures variety is the competition of crystals with different dispersity, when a field of invariant reaction is divided into the fragments with the tiny eutectical crystals, with more large primary crystals and with the both type of these crystals [13].

Acknowledgements

The paper was presented as Plenary Lecture and was published with the permission of ic-cmtp2, the 2nd International Conference on Competitive Materials and Technology Processes, 8-12 October 2012, Miskolc-Lillafüred, Hungary.

References

[1] Taylor, H. F. W.: *Cement Chemistry.* Thomas Telford, London, 1997, 459 p.

[2] Lea, F.: *Lea's Chemistry of Cement and Concrete.* P.C. Hewlett, London, 1998, 1092 p.

[3] De Noirfontaine, M. N. – Tusseau-Nenez, S. – Girod-Labianca, C. – Pontikis, V.: *CALPHAD formalism for Portland clinker: thermodynamic models and databases.* Journal of Material Science 47(3), February 2012, pp 1471-1479, http://dx.doi.org/10.1007/s10853-011-5932-7

[4] Pashchenko, A. A. – Aleksenko, N. V. et al: *Physical Chemistry of Silicates.* Edited by Pashchenko, A. A., Vysshaya Shkola, Kiev, 1977, 368 p. (in Russian)

[5] Lutsyk, V. I. – Zelenaya, A. E. – Savinov, V. V.: *Melt solidification in the ceramic system CaO-Al_2O_3-SiO_2. ICC3: Symposium 8: Glass-Science & Technology and Photonic Applications.* IOP Conference Series: Materials Science and Engineering. 18(2001) 112005, IOP Publishing, http://dx.doi.org/10.1088/1757-899X/18/11/112005

[6] Lutsyk, V. I. – Zelenaya, A. E. – Savinov, V. V.: *Phase trajectories in CaO-Al_2O_3-SiO_2 melts.* Crystallography Reports. 57(7), December 2012, pp. 943-947., http://dx.doi.org/10.1134/S1063774512070176

[7] Gentile, A. L. – Foster, W. R.: *Calcium Hexaluminate and Its Stability Relations in the System CaO-Al_2O_3-SiO_2.* Journal of the American Ceramic Society. 46(2), February 1963, pp. 74-76., http://dx.doi.org/10.1111/j.1151--2916.1963.tb11679.x

[8] Levin, E. M. – Robbins, C. R. – McMurdie, H. F.: *Phase Diagrams for Ceramists.* American Ceramic Society, Ohio, 1964, 395 p.

[9] Toropov, N. A. – Bazarkovsky, V. P. – Lapshin, V. V. et al.: *Diagrams of Silicate Systems.* vol 3. Ternary Silicate Systems, Nauka, Leningrad, 1972, pp. 184-190 (in Russian)

[10] Lutsyk, V. I. – Zelenaya, A.: *Crystallization paths and microstructures in ternary oxide systems with stoichiometric compounds.* Proc. Int. Conf. Oxide Materials for Electronic Engineering (Lviv, Ukraine), 3-7 Sept. 2012, pp. 133-134., http://dx.doi.org/10.1109/OMEE.2012.6464817

[11] Lukas, H. L. – Hengl, E. T. – Petzow, G.: *Zeitschrift für Metallkunde.* 77, pp. 360, 1986

[12] Lutsyk, V. I.: *Bulletin of Buryat Scientific Centre* (SB RAS) no 1(5), 78 p., 2012 (in Russian)

[13] Lutsyk, V. I. – Nasrulin, E. R.: *Competition of primary and eutectic crystals in invariant and univariant reactions.* Crystallography Reports. 57(7), December 2012, pp. 979-983., http://dx.doi.org/10.1134/S1063774512070152

Ref.:
Vasily **Lutsyk** – Anna **Zelenaya**: *Crystallization paths in SiO_2-Al_2O_3-CaO system as a genotype of silicate materials.*
Építőanyag, 65. évf. 2. szám (2013), 34–38. p.
http://dx.doi.org/10.14382/epitoanyag-jsbcm.2013.7

Kristályosodási folyamatok a SiO_2-Al_2O_3-CaO anyagrendszerben, mint a szilikát anyagok genotípusában

A SiO_2-Al_2O_3-CaO anyagrendszerben a nem elegyedő folyadékfázisok mezőjéből kiindulva a krisztobalit (SiO_2 cr), a tridimit (SiO_2 tr) és a mullit ($3Al_2O_3$ x $2SiO_2$) fázisátalakulása – kristályosodása – kerül a szerzők által bemutatásra a T-x-y koordináta rendszerben számítógépes modellezés segítségével. Az elvégzett számítógépes modellezés és elemzés eredményeként feltárulnak azok a hőmérséklettől és összetételtől függő unikális mikro-szerkezettel bíró terek és mezők, amelyekben a szilikát anyagok genotípusát alkotó anyagrendszerben az egyes komponensek kristályosodási folyamata nem önállóan megy végbe.
Kulcsszavak: fázisdiagram, kristályosodás, SiO_2-Al_2O_3-CaO rendszer, számítógépes modellezés

NIISK, the Ukrainian state agency "Research Institute of Building Constructions" celebrates its 70th anniversary in 2013

The Institute was founded in 1943 by the Council of People's Commissars of the USSR on October 26, 1943 and received the name "Ukrainian Research Institute facilities (UkrNDIS)" from the temporary location of the Institute in Moscow. The main purpose of the institute was the development and implementation of advanced building science and technology, conduct research on housing and civil engineering and technical assistance to construction companies. The main activity of the Institute was to address a number of issues in the construction industry, contributing to the implementation of the program of construction of recovery in short term construction projects destroyed during the 2nd World War and find the most efficient design, saving in building materials and replacement techniques. The UkrNDIS was transferred to Kyiv in March 1944.

During the years of its history NIISK solve complex scientific and technical issues concerning the construction of many buildings in Ukraine and other former Soviet republics. Numerous research and development institute were used in our country and abroad. Scientists and engineers have created a unique institute of technology and building construction in the Ukraine and other former Soviet republics and make several housing estates in difficult geological conditions. NIISK is now a large research centre known not only in Ukraine but also abroad. The work of the institute has been recognized by international prizes and honours.

Over 500 specialists are currently working for the institute, which has branches and branch laboratories in several regions of Ukraine. Main Technical Committees of NIISK: Energy Efficiency of buildings; Building construction; Protection of buildings. In addition to scientific departments, the institute has design departments and experimental bases developing projects and technologies for new structural designs and producing structures for experimental construction.

The institute issues the scientific collection "Building structures" as well as the scientific journal "Geotechnical world".

The institute carries out work in the following areas: building structures, geotechnics and foundation engineering, seismic resistance construction, energy effectiveness and acoustics, reliability and effectiveness of technical decisions, test methods for building structures and scientific support for large structures.

Among other honours, the Institute was awarded with the International Prize for Commercial Prestige – The New Millennium Prize in 2002, and The World Quality Award XXI Century – World of Marketing award in 2003.

Cu-Hf-Al amorphous/nanocrystalline composite particles produced by milling

Mária SVÉDA ▪ Hungarian Academy of Sciences-University of Miskolc, Materials Science Research Group ▪ femmaria@uni-miskolc.hu
Márton BENKE ▪ University of Miskolc, Department of Materials Science, Metal Forming and Nanotechnology ▪ fembenke@uni-miskolc.hu
András ROÓSZ ▪ University of Miskolc, Department of Materials Science, Metal Forming and Nanotechnology ▪ femroosz@uni-miskolc.hu

Érkezett: 2013. 08. 28. ▪ Received: 23. 08. 2013.▪ http://dx.doi.org/10.14382/epitoanyag-jsbcm.2013.8

Abstract
$Cu_{54}Hf_{36}Al_{10}$ amorphous/nanocrystalline composite particles were prepared by ball-milling. Crystalline master alloys were prepared by induction melting under purified argon atmosphere. During the mechanical amorphization the grinded ingots were milled for different durations of time and with several interruptions in order to analyse the structure of the powders. The mechanical milling was performed in a Pulverisette5 high energy planetary ball-mill under argon atmosphere using stainless vial and balls with diameters of about 3 mm, 5 mm and 10 mm. The ball-to-powder ratio was 20:1. The milled powders were analyzed by XRD to determine the amorphous fraction, by SEM to characterize the microstructure and by DSC to observe processes in the powders during heating. After milling for 20 h, an amorphous structure appeared and the amorphous fraction was 95%.
Keywords: amorphisation, milling, planetary ball-mill

Mária SVÉDA
material science engineer, MTA-ME Materials Science Research Group working as a research fellow. In 2007, she obtained a PhD in developed monotectic surface layers of laser surface. The main research area: the crystallization of peritectic alloys.

Márton BENKE
material science engineer, University of Miskolc Physical Metallurgy Metal Forming and Nanotechnology Institute works as a research fellow. In 2010 he obtained a PhD. Main research area: Study of martensite transformations in TRIP / TWIP steels and Cu-based shape memory alloys.

András ROÓSZ
metallurgical engineer, member of the Hungarian Academy of Sciences. Head of MTA-ME Materials Science Research Group. Chairmen of the University of Miskolc, Kerpely Antal Materials Science and Technology Doctoral School. The main research area: solid phase transformation, crystallization, laser surface treatment, space materials science, simulation of transformation, material information.

1. Introduction

The materials of bulk metallic glasses (BMG) attract tremendous attention because they offer unique mechanical properties such as ultrahigh strength or high hardness [1-5]. Copper-based amorphous alloys are particularly interesting for practical applications as new structural materials due to their significant advantages, including their low cost, high fracture strength of around 2 GPa, often coexisting with visible ductility, and feasibility for the formation of BMG based composites [5-10].

The new types of Cu-Hf-Al alloys are suitable structural materials in engineering and motorcar industry owing to their excellent mechanical properties such as strength as well as corrosion and wear resistance. The $Cu_{49}Hf_{42}Al_9$ alloy was developed by Jia et al. [6] and shows a critical diameter value higher than the values obtained earlier, that is, it can be cast in a bulk amorphous form with a diameter of 10 mm. Ball-milling (BM) is a well-known process producing a wide range of materials with unique properties [12].

The present work reports about $Cu_{54}Hf_{36}Al_{10}$ amorphous/nanocrystalline composite particles prepared by ball-milling.

2. Experimental

The crystalline master alloys were prepared by induction melting under purified argon atmosphere. The master alloy ingots were grinded to particles with size below 320 μm before the mechanical milling. The particles were milled for different periods of time during the mechanical amorphization.

The procedure was interrupted after arbitrarily selected milling times in order to analyze the structure of the powders. The mechanical milling was performed in a Pulverisette 5 high-energy planetary ball-mill under argon atmosphere using stainless steel vial and balls with diameters of 3 mm, 5 mm and 10 mm. The ball-to-powder ratio was 20:1. The optimal parameters of the milling were determined in a previewed work of the Materials Science Research Group [1-2].

The microstructure of the powders was characterized using a 1830 I Amray Scanning Electron Microscope equipped with an EDX DX4 and a Zeiss EVO MA Scanning Electron Microscope. The ball-milled powders were analyzed by X-ray diffraction (XRD) using a Philips PW 1830 diffractometer with Cu Kα radiation (λ = 0.1542 nm). The glass transition and crystallization temperatures of the amorphous phase were measured with a Netzsch 204 DSC with alumina container. The particle size was measured by a Quantimet Image Analyzer using Leica Software.

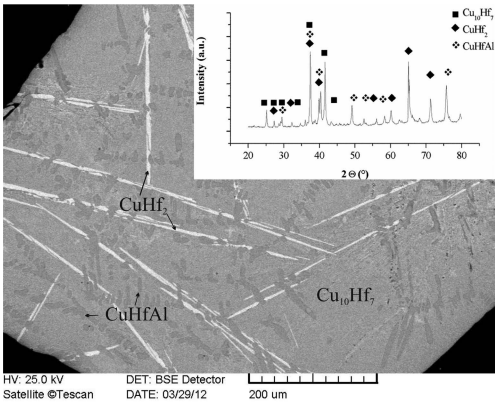

Fig. 1. Backscattered SEM image of the $Cu_{54}Hf_{36}Al_{10}$ master alloy with the XRD diffractogram
1. ábra A $Cu_{54}Hf_{36}Al_{10}$ alapötvözet elektronmikroszkópos képe és röntgendiffraktogramja

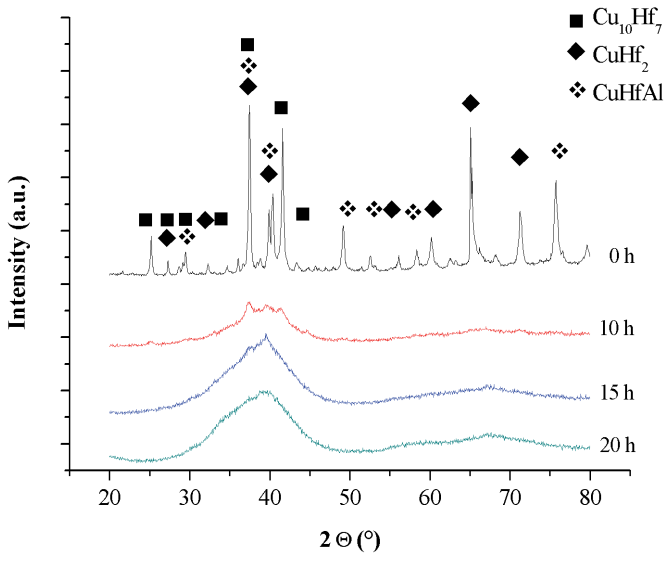

Fig. 2. XRD diffractograms of the $Cu_{54}Hf_{36}Al_{10}$ powders as function of milling time
2. ábra $Cu_{54}Hf_{36}Al_{10}$ porok röntgendiffraktogramjai az őrlési idő függvényében

3. Results and discussion

Figure 1 shows the $Cu_{54}Hf_{36}Al_{10}$ crystalline master alloy with three identified intermetallic compounds: $Cu_{10}Hf_7$ (orthorhombic, a = 1.2587 nm, b = 0.9238 nm, c = 0.9265 nm [13]), $CuHf_2$ (tetragonal, a = 0.3170 nm, c = 1.1133 nm [14]) and the ternary compound CuHfAl (hexagonal, $MgZn_2$-type Laves-phase, a = 0.5155 nm, c = 0.8381 nm [15]). Confirmed by element analysis using EDX, the needle shape crystalline phases (lighter) were identified as $CuHf_2$, the dendrites (dark gray) as CuHfAl and the matrix $Cu_{10}Hf_7$ intermetallic compounds, respectively.

Figure 2 shows the XRD patterns of $Cu_{54}Hf_{36}Al_{10}$ powders after different milling times. 10 h milling resulted in broadening the crystalline diffraction peaks and reduction of their intensity; however, there was no significant change in the position of diffraction peaks. Increasing the milling time beyond 10 hours led to the appearance of a broad diffuse diffraction maximum between 2Θ = 32° and 46°, which implies the formation of an amorphous phase. After milling for 20 h, an amorphous structure appeared and the amorphous fraction was 95%.

The scanning electron images show the structure of the $Cu_{54}Hf_{36}Al_{10}$ powders as a function of milling time (Figure 3). After 10 hours milling $CuHf_2$ phase remains in the powder, as seen in Figure 3 (a). Figure 3 (b) shows 15 hours milled powder. The needle shape crystalline phases (lighter) were identified as $CuHf_2$. The particles are coalescent with gaps encompassed between them. Figure 3 (c) shows 20 h milled powder in lower magnification, while Figure 3 (d) – in higher magnification. The structure of the particles can not be observed, an amorphous structure appears and the amorphous fraction is 95% During the high-energy milling the particles were repeatedly attended, cold welded, fractured and rewelded. Figure 4 shows the $Cu_{54}Hf_{36}Al_{10}$ particle size distribution as a function of milling time measured by Quantimet Image Analyzer. The average size of the particles decreases with increaseing milling time. The majority of the particles in the starting powder were 200 μm in size. As the milling time increases, the range of particles size distribution narrows. While the average particle size in the starting powder was 200 μm, after 20 hours of milling it was only ~ 10 μm.

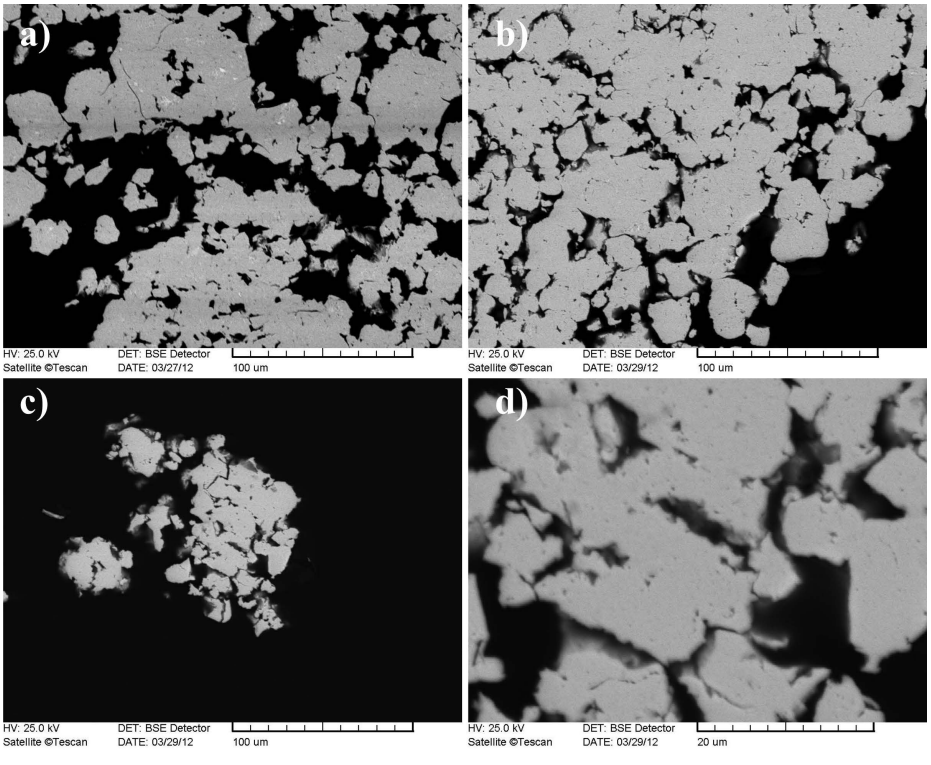

Fig. 3. Backscattered SEM images of the $Cu_{54}Hf_{36}Al_{10}$ powder as function of milling time: a) 10 h, b) 15 h, c) 20 h, d) the same as c) in higher magnification
3. ábra $Cu_{54}Hf_{36}Al_{10}$ porok elektronmikroszkópos képei az őrlési idő függvényében: a) 10 h, b) 15 h, c) 20 h, d) 20 h, nagyobb felbontású képen

Thermal data of the $Cu_{54}Hf_{36}Al_{10}$ alloy were obtained by DSC measurements with the first crystallization temperature at Tx = 572 °C and the crystallization peak temperature being at Tp = 618 °C.

4. Conclusions

Within the frames of this work $Cu_{54}Hf_{36}Al_{10}$ powders were produced by ball-milling with the milling time varying between 5 and 20 h.

The results can be summarized as follows: increasing the milling time resulted in an increase of the amorphous fraction. After milling for 20 h, an amorphous structure appeared and the amorphous fraction was 95%. Thermal data of the $Cu_{54}Hf_{36}Al_{10}$ alloy were obtained by DSC measurements with the first crystallization temperature at Tx = 572 °C and the crystallization peak temperature being at Tp = 618 °C.

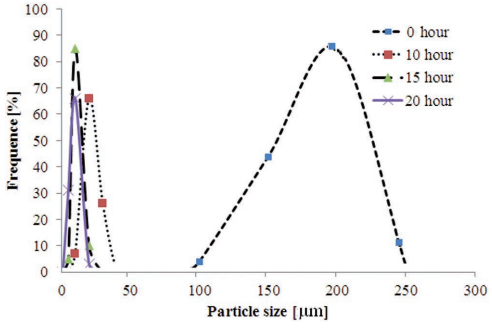

Figure 4. $Cu_{54}Hf_{36}Al_{10}$ *particle size distribution*
4. ábra $Cu_{54}Hf_{36}Al_{10}$ *szemcseméret eloszlás*

Acknowledgements

This work has been carried out as part of the TÁMOP-4.2.1.B-10/2/KONV-2010-0001 project within the framework of the New Hungarian Development Plan. The realization of this project is supported by the European Union, co-financed by the European Social Fund.

The paper was presented as Poster + Short oral presentation and was published with the permission of ic-cmtp2, the 2nd International Conference on Competitive Materials and Technology Processes, 8-12 October 2012, Miskolc-Lillafüred, Hungary.

References

[1] Tomolya K. – Janovszky D. – Sveda M. – Hegman N. – Solyom J. – Roosz A.: *CuZrAl Amorphous Alloys Prepared by Casting and Milling.* Journal of Physics: Conference Series. **144**(1), 2009: pp. 012032 1-5. http://dx.doi.org/10.1088/1742-6596/144/1/012032

[2] Tomolya K. – Janovszky D. – Janvari T. – Sycheva A. – Tranta F. – Solyom J. – Ferenczi T. – Roosz A.: *Consolidation of* $Cu_{58}Zr_{42}$ *amorphous/nanocrystalline powders by PM.* Journal of Alloys and Compounds. **536**(1), 25 September 2012, pp. S154-S158., http://dx.doi.org/10.1016/j.jallcom.2011.12.107

[3] Zhang, W. – Inoue, A.: *Thermal Stability and Mechanical Properties of Cu-Based Bulk Glassy Alloys in* $Cu_{50}(Zr_{1-x}Hf_x)_{45}Al_5$ *System.* Materials Transactions, **44**(10), 2003, pp. 2220-2223.

[4] Jia, P. – Xu, J.: *Comparison of bulk metallic glass formation between Cu-Hf binary and Cu-Hf-Al ternary alloys.* Journal of Materials Research. **24**(1), 2009 No. 1, pp. 96-106., http://dx.doi.org/10.1557/JMR.2009.0014

[5] Jia, P. – Zhu, Z-D. – Zuo, X-W. – Wanga, E-G. – He, J-C.: *Investigations of compressive strength on Cu-Hf-Al bulk metallic glasses: Compositional dependence of malleability and Weibull statistics.* Intermetallics **19**(12), December 2011, pp. 1902–1907., http://dx.doi.org/10.1016/j.intermet.2011.07.031

[6] Jia, P. – Guo, H. – Li, Y. – Xu, J. – Ma, E.: *A new Cu–Hf–Al ternary bulk metallic glass with high glassforming ability and ductility 2006.* Scripta Materialia **54**(12), June 2006, pp. 2165–2168. http://dx.doi.org/10.1016/j.scriptamat.2006.02.042

[7] Cai, A-H. – Xiong, X. – Liu, Y. – Zhou, Y. – An, W-K. – Luo, Y.: *Regular Cu based amorphous alloy powder.* Journal of Alloys and Compounds **497**(1-2), 14 May 2010, pp. 234-238., http://dx.doi.org/10.1016/j.jallcom.2010.03.018

[8] Wang, Y-Y. – Bian, X-F. – Ran, J.: *Effects of cooling rate on thermal expansion of* $Cu_{49}Hf_{42}Al_9$ *metallic glass.* Transactions of Nonferrous Metals Society of China **21**(9), September 2011, pp. 2031–2036. http://dx.doi.org/10.1016/S1003-6326(11)60968-0

[9] Madge, S. V. – Wada, T. – Louzguine-Luzgin, D.V. –Greer, A.L. – Inoue, A.: *Oxygen embrittlement in a Cu–Hf–Al bulk metallic glass.* Scripta Materialia **61**(5), September 2009, pp. 540–543. http://dx.doi.org/10.1016/j.scriptamat.2009.05.018

[10] Maddala, D. – Hebert, R. J.: *Effect of notch toughness and hardness on sliding wear of* $Cu_{50}Hf_{41.5}Al_{8.5}$ *bulk metallic glass.* Scripta Materialia **65**(7), October 2011, pp. 630–633., http://dx.doi.org/10.1016/j.scriptamat.2011.06.046

[11] Choi-Yim, H.: *Thermal and Elastic Properties of Cu-Hf-Al Bulk Metallic Glasses.* Journal of the Korean Physical Society **60**(3), February 2012, pp. 485-487., http://dx.doi.org/10.3938/jkps.60.485

[12] Inoue, A. – Zhang. W.: *Bulk glassy Cu-based alloys with a large supercooled liquid region of 110 K.* Applied Physics Letters **83**(12), 2003, 2351-2353., http://dx.doi.org/10.1063/1.1613813

[13] Bsenko, L.: *Crystallographic data for intermediate phases in the copper-zirconium and copper-hafnium systems.* Journal of the Less Common Metals **40**(3), May 1975, pp. 365–366., http://dx.doi.org/10.1016/0022-5088(75)90085-5

[14] JCPDS 1995No. 18-0440. International Center for Diffraction Data: Newton Square, PA

[15] Handbook of Ternary Alloy Phase Diagrams, edited by P. Villars, A. Prince, and H. Okamoto (ASM International Publishing, (1995), p. 3219.

Ref.:
Mária **Svéda** – Márton **Benke** – András **Roósz**: *Cu-Hf-Al amorphous/nanocrystalline composite particles produced by milling*
Építőanyag, 65. évf. 2. szám (2013), 39–41. p.
http://dx.doi.org/10.14382/epitoanyag-jsbcm.2013.8

Cu-Hf-Al amorf/nanokristályos szerkezetű por előállítása őrléssel

$Cu_{54}Hf_{36}Al_{10}$ amorf/nanokristályos szerkezű port állítottunk elő golyós malomban. Kristályos mesterötvözetet készítettünk indukciós olvasztás alatt argon atmoszférában. Az őrléshez Fritsch által gyártott Pulverisette 5 golyósmalmot használunk, amelybe golyókat tettünk, amelyek átmérője 5, 7 és 10 mm volt. Argonnal feltölthető, saválló acél tégelybe saválló acélból kísérletezve 20:1 golyó/őrlendő anyagaránnyal dolgoztunk. Az őrölt porok szerkezetét röntgendiffrakciós (XRD) vizsgálatokkal tanulmányoztuk és meghatároztuk a fázisokat illetve az amorf térfogathányadot. A mikroszerkezet jellemzésére pásztázó elektronmikroszkópos (SEM) vizsgálatokat alkalmaztunk. 20 órás őrlést követően a kapott amorf térfogathányad 95%-os volt.
Kulcsszavak: amorfizálás, őrlés, golyós malom

The approximate calculation of the MgO rich corner of the $MgO-Al_2O_3-CaO-SiO_2$ phase diagram by ESTPHAD method

Tamás MENDE
metallurgical engineer (2005), PhD (2010), Pro Scientia Gold Medalist (2005). The main research field: equilibrium phase diagram calculation in cases of binary, ternary and quaternary oxide and metallic systems.

András ROÓSZ
metallurgical engineer, member of the Hungarian Academy of Sciences. Head of MTA-ME Materials Science Research Group. Chairmen of the University of Miskolc, Kerpely Antal Materials Science and Technology Doctoral School. The main research area: solid phase transformation, crystallization, laser surface treatment, space materials science, simulation of transformation, material information

Tamás MENDE ▪ Hungarian Academy of Sciences-University of Miskolc, Materials Science Research Group ▪ tamas.mende@uni-miskolc.hu
András ROÓSZ ▪ University of Miskolc, Department of Materials Science, Metal Forming and Nanotechnology ▪ femroosz@uni-miskolc.hu

Érkezett: 2013. 09. 02. ▪ Received: 02. 09. 2013. ▪ http://dx.doi.org/10.14382/epitoanyag-jsbcm.2013.9

Abstract
The ESTPHAD (Estimation of Phase Diagrams) thermodynamically based phase diagram calculation method was developed by us in the University of Miskolc. The paper shows the writing up by ESTPHAD method of the MgO rich corner of the binary, ternary and quaternary phase diagrams of the $MgO-Al_2O_3-CaO-SiO_2$ oxide system. The differences between the calculated data and data from literature are less than 1% of the liquidus temperature values, which is near equal to the measurement error of the high temperature measuring.
Keywords: equilibrium phase diagram calculation, ESTPHAD method, oxide system

1. Introduction

In case of ceramic industries it is very important to know the liquidus temperature of multicomponent oxide system. By using of the ESTPHAD method the liquidus and solidus curves (binary systemí) or surfaces (multicomponent system) of the equilibrium phase diagrams can be calculated by simple equations. The ESTPHAD method has thermodynamic based equations and hierarchical structure. Used to the hierarchical structure, it is possible to approach the ternary liquidus surface (in case of high MgO concentration) on the basis of the binary phase diagrams even if the ternary system is not known. For the calculations we can use measured or calculated data from literature and with regression analysis we can determine easily the constants of the equations.

2. Calculation of liquidus temperature

The equation used in ESTPHAD method (Eq. 1) is based on thermodynamic principles. In equilibrium the partial molar free energy of the phases being in equilibrium are equal. After a long deduction [1,2], the liquidus temperature can be calculated as follows in case of binary A-B system:

$$T_L = \frac{T_0}{1+\sum_{i=1}^{\infty} A(i:0:0)(c_B)^i} = \frac{T_0}{1+F_{AB}(c_B)} \quad (1)$$

Where: T_0 melting point of pure element (K), c_B liquid phase concentration (wt%), A(i:0:0), *A(0:j:0) and A(0:0:k)* calculated coefficients, $F_{AB}(c_B)$ polynome which belongs to liquidus concentration.

The ESTPHAD algorythm has hierarchical structur, which means that we are able to use the calculated polynomes of binary systems (created in case of A-B and A-C systems) to approximate the ternary A-B-C liquidus temperature. The results would be more precise used the ΔF_{ABC} function determined from the measured or calculated ternary equilibrium phase diagram *(Eq.2.)*.

$$T_L = \frac{T_0}{1+F_{AB}(c_B)+F_{AC}(c_C)+\Delta F_{ABC}(c_B;c_C)} \quad (2)$$

The ΔF_{ABC} function includes mixed products of the concentrations of the components with sufficient powers:

$$\Delta F_{ABC}(c) = A(1;1;0)\cdot(c_B)\cdot(c_C) + A(2;1;0)\cdot(c_B)^2\cdot(c_C) + A(1;2;0)\cdot(c_B)\cdot(c_C)^2 + \ldots$$

$$= \sum_{i,j=1-\ldots} A(i;j)\cdot(c_B)^i\cdot(c_C)^j \quad (3)$$

The calculation of the liquidus temperature of quaternary system and the FABCD function can be set up by the aforementioned hierarchical way (Eq.4, Eq.5):

$$T_L = \frac{T_0}{1+F_{AB}+F_{AC}+F_{AD}+\Delta F_{ABC}+\Delta F_{ABD}+\Delta F_{ACD}+\Delta F_{ABCD}(c_B;c_C;c_D)} \quad (4)$$

$$\Delta F_{ABCD}(c) = A(1;1;1)\cdot(c_B)\cdot(c_C)\cdot(c_D) + A(2;1;1)\cdot(c_B)^2\cdot(c_C)\cdot(c_D) + \ldots =$$

$$= \sum_{i,j,k=1-\ldots} A(i;j;k)\cdot(c_E)^i\cdot(c_C)^j\cdot(c_D)^k \quad (5)$$

3. Results

The liquidus curves of the binary phase diagrams can be calculated with ±5 K variances (which is less than 0,3% of the liquidus temperature) by the ESTPHAD method. Due to the hierarchical structure of the ESTPHAD method, the liquidus surfaces of the ternary phase diagrams can be approximate with ±25 K difference (less than 1%), the quaternary liquidus temperature (above 80 wt% MgO content) ±25 K difference (less than 1%). On the following figures can be found the digitalized (which were used as base data for our calculations) and calculated liquidus curves and surfaces.

By using our equations and the following calculated coefficients (Table 1. to 3.) the liquidus temperature can be calculated easily. The T_0 initial value in Eq. (1) to (4) is equal to 3083 K.

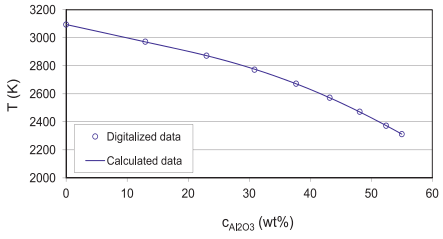

Fig. 1. The digitalized [4] and calculated liquidus curves of MgO phase in case of MgO-Al_2O_3 phase diagram
1. ábra Az MgO fázis digitalizált [4] és számított likvidusz vonala MgO-Al_2O_3 fázisdiagramban

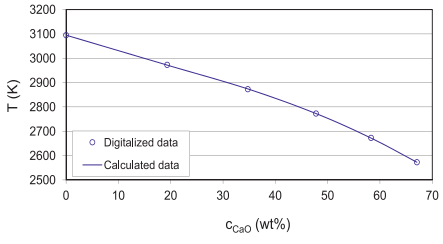

Fig. 2. The digitalized and calculated liquidus curves of MgO phase in case of MgO-CaO phase diagram [4].
2. ábra Az MgO fázis digitalizált és számított likvidusz vonala MgO-CaO fázisdiagramban [4]

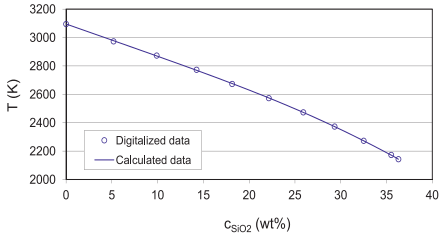

Fig. 3. The digitalized and calculated liquidus curves of MgO phase in case of MgO-SiO_2 phase diagram [3].
3. ábra Az MgO fázis digitalizált és számított likvidusz vonala MgO-SiO_2 fázisdiagramban [3]

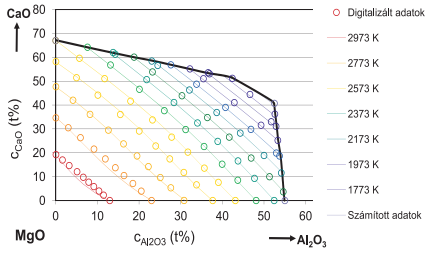

Fig. 4. The digitalized and calculated liquidus surface of MgO phase in case of MgO-Al_2O_3-CaO phase diagram [4].
4. ábra Az MgO fázis digitalizált és számított likvidusz felülete MgO-Al_2O_3-CaO fázisdiagramban [4]

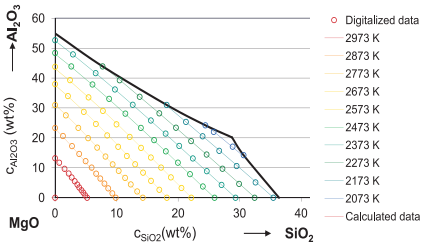

Fig. 5. The digitalized and calculated liquidus surface of MgO phase in case of MgO-Al_2O_3-SiO_2 phase diagram [3].
5. ábra Az MgO fázis digitalizált és számított likvidusz felülete MgO-Al_2O_3-SiO_2 fázisdiagramban [3]

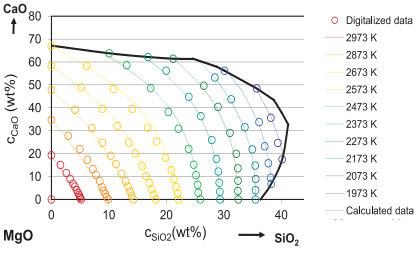

Fig. 6. The digitalized and calculated liquidus surface of MgO phase in case of MgO-CaO-SiO_2 phase diagram [3].
6. ábra Az MgO fázis digitalizált és számított likvidusz felülete MgO-CaO-SiO_2 fázisdiagramban [3]

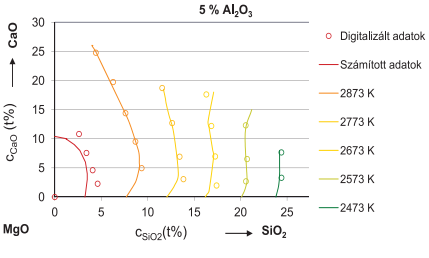

Fig. 7. The digitalized and calculated liquidus surface of MgO phase in case of MgO-CaO-SiO_2 phase diagram and 5% Al_2O_3 section of quaternary system [3].
7. ábra Az MgO fázis digitalizált és számított likvidusz felülete MgO-CaO-SiO_2 fázisdiagramban és a négyfázisú rendszer 5% Al_2O_3 metszete [3]

4. Conclusion

By using the ESTPHAD method we calculated the liquidus temperature of binary, ternary and quaternary systems with a sufficient precision. The differences between the calculated data and data from literature are less than 1%, which is near equal to the measurement error of the high temperature measuring.

Acknowledgements

Our research work was supported by TÁMOP-4.2.1.B-10/2/KONV-2010.

The paper was presented as Poster + Short oral presentation and was published with the permission of ic-cmtp2, the 2nd International Conference on Competitive Materials and Technology Processes, 8-12 October 2012, Miskolc-Lillafüred, Hungary.

References

[1] Roósz, A. – Barkóczy, P. – Farkas, J.: The ESTPHAD: *a Simple Tool for the Simulation of Solidification of Multicomponent Alloys.* SP'07 Proceedings of the 5th Decennial International Conference on Solidification Processing, Sheffield, July 2007, pp. 365-368

[2] Roósz, A. – Kaptay, G. – Farkas, J.: *Thermodynamics-Based Semi Empirical Description of Liquidus Surface and Partition Coefficients in Ternary Al-Mg-Si Alloy,* Materials Science Forum, Volume 414-415 (2003), pp. 323-328. http://dx.doi.org/10.4028/www.scientific.net/MSF.414-415.323

[3] Levin, E.M. – Robins, C.R. – McMurdie, H.F.: *Phase Diagrams for Ceramists,* The American Ceramic Society, 1964, 395 p.

[4] Muan, A. – Osborn, E. F.: *Phase Equilibria Among Oxides in Steelmaking,* Pergamon Press, 1965, 236 p.

Ref.:
Tamás **Mende** – András **Roósz**: *The approximate calculation of the MgO rich corner of the MgO-Al_2O_3-CaO-SiO_2 phase diagram by ESTPHAD method*
Építőanyag, 65. évf. 2. szám (2013), 42–43. p.
http://dx.doi.org/10.14382/epitoanyag-jsbcm.2013.9

A MgO-Al_2O_3-CaO-SiO_2 fázisdiagram MgO-ban dús sarkának közelítő számítása ESTPHAD módszerrel

A kerámiaipari vállalatok számára rendkívül fontos a többalkotós oxid-rendszerek likvidusz hőmérsékletének minél pontosabb ismerete. Az ESTPHAD (Estimation of Phase Diagrams – Fázisdiagramok közelítő számítása) módszerrel két- és többalkotós rendszerek (legyen szó fémes vagy oxid) fázisainak likvidusz hőmérséklete számítható egy egyszerű egyenlet felhasználásával. Az ESTPHAD algoritmusát termodinamikai egyenletekből levezetve hierarchikus módon építettük fel annak érdekében, hogy többalkotós rendszerek számítására is lehetőség nyíljon. A számítások során szakirodalomból származó egyensúlyi fázisdiagramokat használtunk és regressziós analízissel határoztuk meg az ESTPHAD egyenlet paramétereit.
Kulcsszavak: egyensúlyi fázisdiagram számítás, ESTPHAD módszer, oxid-rendszer

Könnyűbetonok koptatóhatással szembeni ellenállása

Dr. NEMES Rita
Okl. építőmérnök,
egyetemi adjunktus
a BME Építőanyagok és
Mérnökgeológia Tanszékén.
Fő érdeklődési területei:
könnyűbeton összetételének tervezése,
könnyűbeton szerkezetek tervezése.
A fib Magyar Tagozat tagja.
Az SZTE Beton Szakosztály tagja.

NEMES Rita ▪ BME Építőanyagok és Mérnökgeológia Tanszék ▪ nemes.rita@gmail.com
Érkezett: 2013. 06. 10. ▪ Received: 10. 06. 2013. ▪ http://dx.doi.org/10.14382/epitoanyag-jsbcm.2013.10

Abrasion Resistance of Lightweight Aggregate Concrete
The durability is one of most important requirements of design of concrete and reinforced concrete structures. The abrasion resistance is less known and common, compared to e.g. freeze-thaw attack, but can be important in case of pavements. Lightweight aggregates usually do not have high abrasion resistance. Different behaviour from normal weight concrete was studied for expanded clay and two type of expanded glass aggregate in present studies.
Keywords: lightweight concrete, expanded clay, expanded glass, abrasion resistance
Kulcsszavak: könnyűbeton, duzzasztott agyagkavics, duzzasztott üvegkavics, kopási ellenállás

1. Bevezetés

A tartósság az egyik legfontosabb szempont lett a beton és vasbeton szerkezetek tervezése során. Betonszerkezetek esetén gyakran a szilárdsági és használhatósági határállapotok kevésbé szigorúak, különösen kültéri szerkezetek esetén, mint a tartóssági követelmények. A tartóssági tulajdonságok ellenőrző vizsgálatai közül a fagyállóság a legismertebb. Az EN 206-1:2002 betonszabvány magyar NAD-ja (MSZ 4798-1:2004) a fagyállósági kitéti osztályok mellett tartalmazza a vízzáróság és a kopásállóság vizsgálatát és osztályba sorolását is. Térburkolatok alkalmazásakor nagy jelentősége van a kopásállóságnak. Burkolókövek esetén gyakori ez a vizsgálat, de a beton burkolatok terjedésével, a betonoknál egyre nagyobb szükség van rá. A kopásállóság kérdése ritkán merül föl könnyűbetonok esetén. Éppen ezért kevés adat áll rendelkezésre.

A szakirodalomban elérhető eredmények többnyire ASTM szabvány szerinti vizsgálatok eredményeit tartalmazzák (pl. ASTM C779 / C779M - 12 Standard Test Method for Abrasion Resistance of Horizontal Concrete Surfaces), ahol elsősorban valamilyen benyomódás, bemaródás alapján minősítik a betonokat kopásállóság szempontjából. Ilyen vizsgálattal svéd kutatók Leca (duzzasztott agyagkavics) adalékanyagos betonon (testsűrűség: 1750 kg/m^3, nyomószilárdság: 37,0 MPa) jobb kopásállóságot kaptak, mint közel azonos nyomószilárdságú normál beton esetén. A koptatási mélység, vizsgálattól függően, a könnyűbetonokon 64-73% lett a vizsgált normál betonokon mérthez képest [1]. Az ilyen típusú vizsgálatok sok esetben kevés információt nyújtanak az adalékanyagra vonatkozóan, általában a felhasználási terület és a nyomószilárdság irányából közelítik a problémát. Könnyű adalékanyaggal általában azonos szilárdsági osztály mellett nagyobb habarcsszilárdság szükséges, ami szintén befolyásolja a tartóssági vizsgálatok eredményét.

A Magyarországon szokásos, eredetileg kőzetekre kidolgozott Böhme vizsgálattal (MSZ 18260-1:1981) hasonlítottuk össze hagyományos betonok és könnyűbetonok kopással szembeni ellenállóképességét. Ezt a módszert nem csak kőzeteken, hanem térburkoló- és pályabetonokon is alkalmazzák. A kutatásunk során gyenge habarcsminőségeket választottunk, hogy elsősorban az adalékanyag legyen a meghatározó, mivel a betonok kopásállósága a szakirodalmi adatok és szabványok szerint elsősorban az adalékanyagtól és annak kopásállóságától függ. Az MSZ 4798-1 elő is írja, hogy milyen adalékanyagok alkalmazhatók kopásálló betonokhoz (ezek között nem szerepel a könnyű adalékanyag). Előfordulnak esetek, amikor viszont nem a kopásállóság az elsődleges jellemző, amit a betonnak teljesítenie kell, viszont ki lesz téve koptatási igénybevételnek. Ilyen volt például a budapesti Margit híd felújítása során alkalmazott ideiglenes pályalemez betonja. A legfontosabb követelmény a testsűrűség volt, amit maximálni kellett teherbírási szempontok alapján (az eredeti terhelés értékét nem volt szabad meghaladni az építés alatt sem). A szilárdsági igény kicsi volt (megfelelt az LC20/22 szilárdsági osztály), de tartóssági szempontból meg kellett felelnie fagyállósági és kopásállósági követelményeknek is. Ezek ugyan csökkentett mértékűek voltak, mivel a szerkezet várható élettartama 1 év volt (a tényleges élettartam pár hónappal kevesebb is). A fagyállóságra vonatkozóan több szakirodalmi adat és saját mérési eredmény is rendelkezésre állt, amely az alkalmazást alátámasztotta, azonban a kopásállóságra vonatkozó ismereteket laboratóriumi vizsgálattal kellett kiegészíteni.

A projekt során szerzett tapasztalatok alapján felmerült, hogy vajon nem a szabványnak megfelelő adalékanyagokkal készülő betonok mennyire felelhetnek meg a kopásállósági követelményeknek, illetve, hogy milyen mértékben eredményez jó kopásállóságot az adalékanyag, a cementkőváz és ezek együttdolgozása.

2. Kísérletek

2.1 Kiindulási adatok, előkísérletek

Az első koptatási kísérletet könnyűbetonon 2009 nyarán végeztük, amikor igazolnunk kellett, hogy a Margit híd ideiglenes pályalemeze készülhet olyan könnyűbetonból, amelynek a testsűrűsége 1600 kg/m^3 alatt marad, de a tervezett 1 éves élettartam alatt megfelelően kopásálló lesz, a gumikerekes járműforgalomnak kitett pályaburkolat betonjaként.

Könnyűbetonokat koptatásnak kitett felületen ritkán alkalmaznak, mert a legtöbb könnyű adalékanyag rossz kopásállóságú. Összehasonlító vizsgálatot végeztünk annak megállapítására, hogy egy közel azonos cementkő vázzal rendelkező kvarckavics és duzzasztott agyagkavics adalékanyagú beton milyen koptatási ellenállással rendelkezik.

Ha a betontól a koptatással szembeni ellenállást követelünk meg (XK1(H), XK2(H), XK3(H), XK4(H)) akkor az MSZ 4798-1 szerint a beton kopásállóságát legalább 28 napos korában, az MSZ 18290-1:1981 szabvány szerinti Böhme-féle eljárással kell

vizsgálni, és a MÉASZ ME-04.19:1995 műszaki előírás 9. fejezet, 9.6.2. szakaszában leírtakat is ajánlatos figyelembe venni. A ΔV térfogatveszteséget mm³-ben kapjuk meg, a következők szerint:

$$\Delta V = \left(1 - \frac{G'}{G}\right) \cdot V$$

ahol ΔV = a próbatest térfogatvesztesége, mm³-ben
G = a próbatest tömege koptatás előtt, g-ban
G' = a próbatest tömege koptatás után, g-ban
V = a próbatest térfogata koptatás előtt, mm³-ben

A koptatást szárazon (légszáraz próbakockákon) és vizesen (vízzel telített próbakockákon és a koptatótárcsára víz csöpögtetése közben) is el kell végezni, és ezek eredményei közül a kedvezőtlenebb a mértékadó vizsgálati eredmény (a határértékeket az *1. táblázat* tartalmazza). Például, ha egy beton kopási vesztesége szárazon 9600 mm³, vizesen 17400 mm³, akkor környezeti (igénybevételi) osztálya: XK2(H). Ennek a táblázatnak a kiegészítésére már elkészült egy javaslat, amelyben egy 5. különlegesen kopásálló osztály is szerepel és nem csak a koptatási határértékek vannak megadva, hanem nyomószilárdsági osztály, cementtartalom, maximális víz-cement tényező és megengedett levegőtartalom is [2].

A ΔV kopási térfogatveszteség megengedett mértéke mm³-ben		
Környezeti (igénybevételi) osztály	Száraz koptatás esetén	Vizes koptatás esetén
XK1(H)	14000	21000
XK2(H)	12000	18000
XK3(H)	10000	16000
XK4(H)	8000	14000

1. táblázat MSZ 4798-1 NAD 5.4. jelű táblázata: Követelmény a beton kopásállóságára
Table 1. Requirements for the abrasion resistance of concrete according to MSZ 4798-1 Table NAD 5.4.

1. ábra Próbatestek a koptató vizsgálat után
Fig. 1. Specimens after the abrasion test

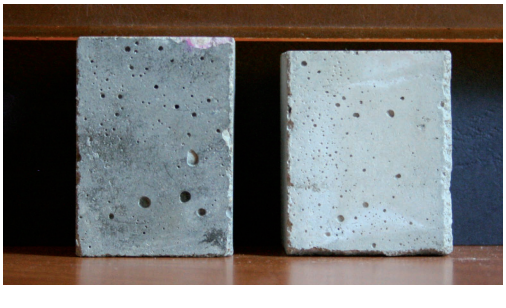

2. ábra Próbatestek a koptató vizsgálat után
Fig. 2. Specimens after the abrasion test

A pontos receptúra ismerete nélkül, illetve idő hiányában nem tudtuk a szabványos vizsgálatot elvégezni az előkísérletek során. Korábban más célra készült, a fent említetteknek megfelelő paraméterekkel rendelkező próbatesteket vizsgáltunk. Ezek 40×40×160 mm-es hasábok voltak, így nem tudtuk a szabványos 70×70 mm-es felületet sem előállítani, ezért 40×40 mm-es felületen végeztük a koptató vizsgálatot. A könnyűbeton duzzasztott agyagkavics adalékanyagú, 1850 kg/m³ testsűrűségű, LC25/28 szilárdsági osztályú volt, a hagyományos beton közel azonos péptartalmú, C40/50 szilárdsági osztályú volt. Mivel a próbatest méretéből adódóan a koptatási felület kisebb volt így azonos erő mellett a koptatás kb. háromszoros intenzitással ment végbe, ezért a 16 szokásos sorozat helyett 5-öt (5×3=15) végeztünk. A kopási térfogatveszteség mértékéből megállapítható volt, hogy a hagyományos beton megfelel a legszigorúbb XK4(H), a könnyűbeton pedig az XK3(H) osztályoknak. A vizsgált könnyűbetonok kopásállósága csak kb. 25%-kal volt rosszabb (*2. ábra*), mint a vizsgált hagyományos betoné. Előnyként említhető, hogy a jobb adalékanyag–cementkő kapcsolat miatt a koptatás során a könnyű adalékanyag szemek nem peregtek ki a koptatott felületből (*1. ábra*) [3].

2.2 Kísérleti terv

A betonösszetételek megtervezésénél a legfontosabb szempont a habarcsváz azonossága volt, hogy a vizsgálat során meghatározott különbségek – amennyire lehetséges – az adalékanyagra vonatkozzanak. Így a testsűrűségi vagy szilárdsági adatok alapján a vizsgált betonok nagyon különbözőnek tűnnek, de a különbséget csak az adalékanyag jellemzői okozzák. CEM I 42,5 N jelű cementtel dogoztunk, a cementadagolás 360 kg/m³ volt, minden alkalmazott adalékanyag esetén enyhén pép-túltelített betont szerettünk volna elérni, hogy a könnyűbetonra jellemző teherbírási viszonyok létrejöhessenek, viszont nagy víz-cement tényezőt (v/c=0,61) alkalmaztunk, hogy a habarcs szilárdsága minél kevésbé legyen mértékadó, ezért finomrészt (140 kg/m³ mészkőliszt adagolást) is alkalmaztunk. Azonos összetétel mellett más jellemzőket is vizsgáltunk, így több szempont alapján optimalizáltuk a kísérleti tervben a betonösszetételt (*2. táblázat* tartalmazza az etalon (kvarckavics adalékanyagos) beton összetételét. A könnyűbetonokat a *2. táblázatban* ismertetett összetétellel készítettük, a változó paraméter csupán a durva adalékanyag frakció volt. A 4 mm feletti adalékanyag frakciókat cseréltük ki a könnyű adalékanyagra. A kutatás során több gyártótól származó, különböző könnyű adalékanyagokat vizsgáltunk meg (*3. táblázat*). Az adalékanyag-jellemzőket az MSZ EN 13055-1:2003 alapján határoztuk meg. A könnyű adalékanyagot mindig száraz állapotban adtuk hozzá a betonkeverékhez. A keverés és bedolgozás során a fél órás vízfelvételnek megfelelő vízmennyiséget az adalékanyag képes elszívni a keverővízből, ettől a beton tényleges víz-cement tényezője és konzisztenciája megváltozna, ezért ezt a vízmennyiséget a keverővízhez hozzáadtuk.

A kopásállósági vizsgálatokhoz 70×70×250 mm-es hasábokat készítettünk és ebből a megszilárdulás után vágással alakítottuk ki a szükséges 70 mm élhosszúságú kockákat. Minden próbatestből több kockát alakítottunk ki, így lehetőségünk volt mind a bedolgozási, mind a vágott felület vizsgálatára. A tartóssági vizsgálatokat szokás vágott felületen végezni, viszont itt a gyakorlati felhasználás szempontjából fontos volt

a valóságban is igénybe vett bedolgozási felület vizsgálata is. A vizsgált betonok nyomószilárdsága egyenesen arányos a testsűrűségükkel (*3. ábra*), tehát ideális arra, hogy ténylegesen az adalékanyagok okozta különbségek hatását vizsgáljuk. A vizsgált betonok testsűrűségét és nyomószilárdságát (28 napos kockaszilárdság) a *4. táblázat* foglalja össze.

	kg/m³	l/m³
cement	360	116,1
finomrész	140	51,9
víz	220	220
folyósítószer	0,36	0,36
adalékanyag 4/8	486	181,9
adalékanyag 8/16	397	148,8
homok 0/4	720	271,7
levegő	-	9,2
Σ	2323	1000

2. táblázat A kísérletek során alkalmazott etalon keverék [4]
Table 2. Reference mix used in the experiments [4]

Adalékanyag	Szemcse-testsűrűség [kg/m³]	Vízfelvétel [m%]		
		0,5 órás	24 órás	teljes
kvarckavics	2670	0	0	0
duzzasztott üvegkavics 1	1320	1,4	1,8	4
duzzasztott üvegkavics 2	949	6,1	8,2	25
duzzasztott agyagkavics	1247	8,0	13,0	21

3. táblázat A kísérletek során alkalmazott adalékanyagok egyes jellemzői [5]
Table 3. Physical properties of the aggregates used in the experiments [5]

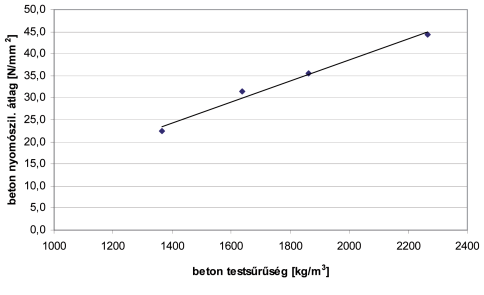

3. ábra A vizsgált betonok nyomószilárdság – testsűrűség összefüggése
Fig. 3. Compressive strength vs. body density responses of the tested concretes

A különböző szabványok és ajánlások szerinti koptatási módok több helyen is eltérnek egymástól. A Böhme módszer szerinti koptatásnál 22 fordulatnyi koptatás után a próbatestet el kell fordítani 90 fokkal és tovább kell koptatni a felületet 22 fordulaton keresztül és így tovább mind a négy él felől. Egy ilyen 4×22 fordulatos sorozatot kell négyszer ismételni az MSZ 18290 szerint. Jelenleg ez a koptatási módszer érvényes mind kőzetekre, mind betonokra (az MSZ 4798 és az MSZ 18290 erre hivatkozik). Betonok esetén korábban az MSZ 4715 szabvány 4×110=440 fordulatos koptatást írt elő (ami megfelel 5×4×22=440 fordulatnak). A MÉASZ ajánlás alapesetben vágott felületeken végzett koptatást javasolt (esetleg előkoptatott felületen). A korábban érvényes MSZ 4715 pedig kihangsúlyozta, hogy a későbbi igénybevételnek megfelelő felületet kell koptatni (és ez jellemezően nem egy vágott, hanem leggyakrabban a bedolgozási felület). A lényeges probléma ezekkel a különböző vizsgálati módokkal az, hogy bár a vizsgálati módok több ponton eltérnek egymástól egyféle kiértékelés használatos (a MÉASZ szerinti) mindegyik esetre.

A vizsgálatnak létezik száraz és nedves változata, így a későbbi használatra jellemző koptatást kell figyelembe venni vagy mindkét módszert el kell végezni és a kedvezőtlenebb alapján kell a kiértékelést végezni. A kísérletek során mi szárazon végeztünk koptatást. Mind vágott, mind bedolgozási felületen elvégeztük a vizsgálatot 5 db 4×22 fordulatos koptatással és minden 4×22 fordulatot követően megmértük a magasságcsökkenést és a tömegveszteséget is.

Adalékanyag	Beton testsűrűség [kg/m³]	Nyomószilárdság [N/mm²]
duzzasztott üveg 2.	1367	22,4
duzzasztott üveg 1.	1637	31,5
duzzasztott agyagkavics	1862	35,5
kvarckavics	2266	44,4

4. táblázat A vizsgált betonok adalékanyaga, testsűrűsége és nyomószilárdsága (28 napos átlagérték)
Table 4. Body density and compressive strength of the concretes tested (28 days age values)

3. Eredmények

A gyakorlatban leggyakrabban előforduló, igénybevett (azaz a bedolgozási) felületen végzett (a *4.* és *5. ábrán* üres jelölőkkel és szaggatott vonallal jelölt) koptatás eredményei alapján megállapítható, hogy a könnyű-adalékanyagos betonok koptatási veszteségе átlagosan kb. háromszorosa a kvarckavics adalékanyagos etalon beton koptatási veszteségének. A vizsgált (tartószerkezeti célra is megfelelő, viszonylag nagy szemcse-testsűrűségű és halmaz-önszilárdságú) könnyű adalékanyagok alkalmazása esetén a kopásállóság lineárisan nő a testsűrűség növekedésével. Az első koptatási sorozat (4×22 fordulat) során kb. 25–50%-kal nagyobb a koptatási térfogatveszteség, mintha arányosan vesszük a 4 és 5 koptatási ciklus eredményét. Kisebb szemcse-testsűrűségű adalékanyagok esetén nagyobb ez az arány. Ha ezt az eredményt összehasonlítjuk a koptatási veszteséggel (azaz gyakorlatilag a próbatest magasságcsökkenésével) akkor látható, hogy ott még nagyobb a különbség. Ennek az az oka, hogy bár a szabványos (*4. ábrán* látható) jellemzőt koptatási térfogatveszteségnek nevezzük, a valóságban tömegveszteség mérésből számítással határozzuk meg. A könnyű adalékanyagos betonok bedolgozási felülete pedig rendszerint nem péptelített, hanem a könnyű adalékanyag szemcsék kismértékben felúsznak a felületre, itt a tömegmérés alkalmazása nem ideális a nem teljesen egyenletes testsűrűség-eloszlás miatt.

A (*4.* és *5. ábrán* kitöltött jelölőkkel és folytonos vonallal jelölt) vágott felületek vizsgálatának eredményei eltérnek a bedolgozási felületen megfigyelt tendenciákhoz képest. Az 1. jelű duzzasztott üvegkaviccsal készült könnyűbeton (ρ_T=1637 N/mm²) vágott felületén vizsgálva lényegesen kedvezőbb kopási ellenállást mutat, mint a bedolgozási felületen vizsgálva. Ez igaz, mind a koptatási térfogat veszteség, mind a koptatási veszteség (magasság csökkenés) értékére. Ezt az adalékanyagot (duzzasztott üvegkavics 1.) kis vízfelvételre optimalizálták a gyártás során. Ennek hatására egy zárt réteg képződött az adalékanyag szemcsék felületén a forgókemencés égetés során. A *3. táblázat* adataiból látható, hogy lényegesen kisebb ennek az adalékanyagnak a

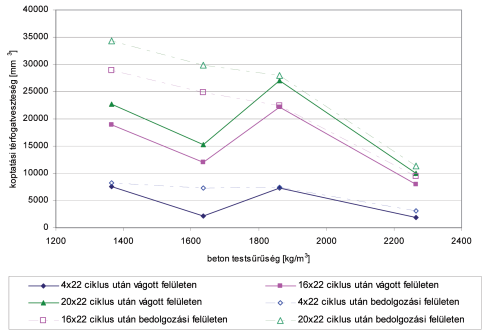

4. ábra A koptatási térfogatveszteség a beton testsűrűségének függvényében (tömegmérésből számítással meghatározott értékek)
Fig. 4. Abrasion volume loss represented as a function of the body density (calculated values from mass measurements)

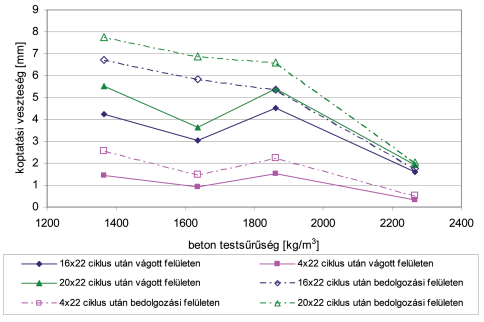

5. ábra A koptatási veszteség (magasság csökkenés) a beton testsűrűségének függvényében
Fig. 5. Abrasion loss (decrease in specimen height) as a function of the body density

vízfelvétele a másik két könnyű adalékanyaghoz képest. A vágott felületen jól látszik, hogy egy külső keményebb réteg képződött, belül pedig vagy a többi könnyű adalékanyagra jellemző porózus rész figyelhető meg, vagy egy kisebb gömb alakú szintén kemény burokkal rendelkező rész (*6. ábra*). Ha a vágott felületen végezzük a koptatást, akkor ezek a külső keményebb részek egyenletesen terhelődnek, így jól ki tudják fejteni a hatásukat, a koptatási veszteség lényegesen kisebb lesz, mint ahol nem ilyen az adalékanyag szerkezete. Bedolgozási felületen nem érzékelhető ez a különbség, ennek az lehet az oka, hogy a legkülső réteg könnyen kopó habarcs, majd egy keményebb burok következik az adalékanyag szemcsén, de ez nagyon kis felületen és nem egyenletesen érintkezik a koptató felülettel, ennek lekopása után pedig vagy a belső puhább rész tud kopni, vagy ahol egy kisebb „gömb" van a belsejében, ez gyakran kihullik. Ez a különbség vizsgálat során is érzékelhető volt, a próbatest sokkal jobban „ugrált" vizsgálat közben, mint a többi összetétel esetén.

6. ábra Az 1. jelű duzzasztott üveg adalékanyagos próbatest vágott felülete koptatás előtt
Fig. 6. Cut surface of the specimen with expanded glass aggregate (specimen no. 1.) before abrasion test

4. Összefoglalás

Összességében elmondható, hogy a könnyű adalékanyagok koptatással szembeni ellenállása valóban kisebb a hagyományos adalékanyagokéhoz képest, azonban ha mégis szükséges, hogy egy könnyűbeton kopásállósági feltételnek is megfeleljen akkor jó habarcsvázra van szükség. A kísérleti eredmények alapján megállapítható, hogy könnyű adalékanyagos betonok esetén nagy jelentősége van annak, hogy a vizsgálatot a tényleges koptatásnak kitett felületen végezzük, mert egyes adalékanyagok esetén lényeges eltérések lehetnek a vágott és a bedolgozott felület eredményei között.

A későbbiekben tervezünk hasonló vizsgálatot végezni többfajta adalékanyag alkalmazása és a zsaluzott felületek koptatása esetére is, további összefüggések keresése érdekében. A későbbi alkalmazások szempontjából fontos lehet azonos adalékanyagok esetén a habarcsváz minőségének javítása és ennek a koptatással szembeni ellenállásra gyakorolt hatásának meghatározása.

5. Köszönetnyilvánítás

Köszönetet mondunk a Duna-Dráva Cement Kft.-nek, a Liabau Kft.-nek és a Geofil Kft.-nek, hogy biztosították számunkra a kísérletekhez szükséges alapanyagokat, illetve Dr. Fenyvesi Olivérnek és Pálinkás Bálintnak (BME) a kísérletek végrehajtásánál nyújtott segítségükért.

Felhasznált irodalom

[1] Chandra, S. –Berntsson, L.: *Lightweight Aggregate Concrete – Science, Technology and Applications.* Elsevier Science, 2002, ISBN 081551820X

[2] Kausay T.: *Betonok környezeti osztályai.* ÉPKO 2009 XIII. Nemzetközi Építéstudományi Konferencia Csíksomlyó, Románia 2009. június 11–14. Szerk.: Köllő G. ISSN 1843-2123 pp. 216-223.

[3] Benedek B. – Józsa Zs. – Nemes R. – Migály B.: *Ideiglenes pályaburkolat a Margit hídon könnyűbetonból.* Beton 18: (7-8) pp 3-8., 2010, ISSN 1218-4837

[4] Fenyvesi O.: *Affect of lightweight aggregate to early age cracking in concrete.* Periodica Polytechnica-Civil Engineering 55:(1) pp. 63-71., 2011, ISSN 1587-3773. http://dx.doi.org/10.3311/pp.ci.2011-1.08

[5] Józsa Zs. – Fenyvesi O.: *Könnyű adalékanyagok belső utókezelő hatása a könnyűbetonok korai zsugorodási repedésérzékenységére.* Szerk.: Köllő G. ÉPKO 2011 XV. Nemzetközi Építéstudományi Konferencia Csíksomlyó, Románia, 2011.06.02-05. ISSN 1843-2123., pp. 124-131.

Hivatkozott szabványok

ASTM C779 / 779CM-12 Standard Test Method for Abrasion Resistance of Horizontal Concrete Surface

MÉASZ ME-04.19:1995 műszaki előírás 9. fejezet Kopásálló betonok

MSZ 4715-4:1987 A megszilárdult beton vizsgálata. Mechanikai tulajdonságok roncsolásos vizsgálata

MSZ 4798-1:2004 Beton 1. rész: Műszaki feltételek, teljesítőképesség, készítés és megfelelőség, valamint az MSZ EN 206-1 alkalmazási feltételei Magyarországon

MSZ EN 13055-1:2003 Könnyű kőanyaghalmazok 1. rész: Könnyű kőanyaghalmazok (adalékanyagok) betonhoz, habarcshoz és injektálóhabarcshoz

MSZ 18290-1:1981 Építési kőanyagok felületi tulajdonságainak vizsgálata. Kopási vizsgálat Böhme módszerrel

Ref.:
Nemes Rita: *Könnyűbetonok koptatóhatással szembeni ellenállása.* Építőanyag, 65. évf. 2. szám (2013), 44–47. p.
http://dx.doi.org/10.14382/epitoanyag-jsbcm.2013.10

Romanesque and Gothic bricks from church in Pác – estimation of the firing temperature

Igor ŠTUBŇA ▪ Dpt. of Physics, Constantine the Philosopher University ▪ istubna@ukf.sk
Rudolf PODOBA ▪ Dpt. of Physics, Faculty of Civil Engineering, Slovak University of Technology ▪ rudolf.podoba@stuba.sk
Peter BAČÍK ▪ Department of Mineralogy and Petrology, Faculty of Natural Sciences, Comenius University ▪ bacik@fns.uniba.sk
Ľuboš PODOBNÍK ▪ Dpt. of Physics, Constantine the Philosopher University ▪ lubos.podobnik@ukf.sk
Érkezett: 2013. 01. 17. ▪ Received: 17. 01. 2013. ▪ http://dx.doi.org/10.14382/epitoanyag-jsbcm.2013.11

Abstract
Pavement bricks taken from the Romanesque and Gothic parts of the church in Pác, in the Trnava County, Slovakia, were investigated by XRD and thermal analyses DTA, TGA and TDA. It was found that the bricks contained dehydroxylated illitic clay, calcite, quartz and feldspar. As revealed, dehydroxylation was completely finished and no rehydroxylation was observed. The estimated firing temperature is between 650 °C and 700 °C. Both bricks were made from local clay and very similar technologies were used.
Keywords: historical ceramics, thermal analysis, firing conditions

Igor ŠTUBŇA
Graduated from Sankt Peterburg Electrotechnical University (1965), major electrophysics – semiconductors and dielectrics. PhD (CSc) degree he earned in Institute of Physics of the Slovak Academy of Sciences (Mechanical properties of the porcelain mixture in dehydroxylation region) in 1980. In the present, he is an associate professor at the Department of Physiscs of the Constantine the Philosopher University, Nitra. The field of research: mechanical and thermophysical properties of electroceramics and building ceramics, measurement methods.

Rudolf PODOBA
Graduated from Constantine the Philosopher University (2009), major materials science. He defended a PhD thesis (DC conductivity of green ceramics during heating up to 1000 °C) in 2013. He is an assistant professor at the Department of Physics, Faculty of Civil Engineering, Slovak University of technology. The field of research: thermal analysis (TGA, DTA), electrical properties of ceramics, historical ceramics.

Peter BAČÍK
Graduated from Comenius University in Bratislava (2003), geology. He defended a PhD thesis (Tourmalinites of Western Carpathians: Chemical Composition and Genetic Aspects) in 2007. He is a senior research fellow at the Department Mineralogy and Petrology, Comenius University in Bratislava. The field of research: crystallography, crystal chemistry of silicates, phosphates and oxides, powder X-ray diffraction

Ľuboš PODOBNÍK
Graduated from Constantine the Philosopher University (2011), major materials science. In the present, he is a PhD student at the Thermophysical Laboratory, Constantine the Philosopher University, Nitra. The field of research: Processes in illite-based and kaolin-based ceramics during firing, historical ceramics.

1. Introduction

Fired bricks, which are manufactured from 4500 BC, are more resistant to harsh weather conditions and much more reliable for use in permanent buildings than sun dried unfired bricks. During the 12th century, fired bricks were reintroduced to Germany from Italy and brickmaking spread also to Hungarian Empire, as confirmed by discovered bricks in Romanesque churches [1, 2]. Investigation of the historic building ceramic objects, such as bricks and tiles, using the physical and chemical methods, helps us to understand the knowledge and skills used to produce them [3]. This is important in the renovation of historic buildings where damaged materials has to be replaced with new ones, with similar properties (e.g. color, texture) to the historic materials. To reveal the basic physical properties of historic building ceramics is beyond the capacity of standard archeological techniques. Therefore, we observe the exploitation of thermal analysis and other methods for better characterization of the archeological findings in the past 40 years (although the first uses of X-ray diffraction analysis (XRD) and differential thermal analysis (DTA) were 70 years ago [4]). Thermal analysis, especially DTA, thermogravimetric analysis (TGA) and thermodilatometric analysis (TDA) may be successfully applied to the study of historic building ceramics [3, 5, 6, 7].

The most frequent object of the thermoanalytical study of historic ceramics is the estimation of the firing temperature. The estimation is based on the comparison of the TGA, DTA and TDA curves measured on the historic ceramic samples with the curves measured on laboratory fired samples [5]. The last are known for the most probable constituents of ceramic clay such as kaolinite, illite, montmorillonite, muscovite, calcite, quartz and feldspar. These minerals will be decomposed and recrystallized, except for feldspar and quartz, if subjected to heating up to 950 °C. This value is around the probable maximum temperature used for the firing of ancient ceramics. Very useful is XRD which helps to identify the presence or absence of these minerals in historic ceramics.

Every method used for the investigation of ancient ceramics, which exploits some kind of thermal analysis, is implicitly based on evaluation of the degree of conversion. It is known that most occurring phyllosilicates in historic ceramics (kaolinite, illite, montmorillonite, muscovite) change irreversibly if heated at a temperature which is within the interval of dehydroxylation of relevant phyllosilicate. Dehydroxylation of these minerals mostly occurs between 400 °C and 600 °C. The upper limit depends on the rate of the heating and size of the fired body. Calcite decomposes according to $CaCO_3 \rightarrow CaO + CO_2$ if heated at the temperatures higher than 700 °C. Both processes, dehydroxylation and decomposition of calcite, are also influenced with a size of the particles, presence of impurities and other.

Dehydroxylation as a characterization of the historical ceramics is not reliable [7]. For example, we can observe dehydroxylation by the help of TGA or DTA if the historical ceramic body was fired at low temperature (e.g. 600 °C) for short time because dehydroxylation was not completed. If the firing temperature was higher (e.g. 700 °C) for sufficient long time, the dehydroxylation was completed. However, dehydroxylation can be also appeared in this case as a result of the escape of rehydroxylated water (originated from hydroxyl groups incorporated into dehydroxylated ceramics) if the historical ceramic body was in a contact with moisture for long time [8]. The products of dehydroxylation can not be considered as irreversible in a span of hundreds or thousands years between the firing and present analyses.

Contrary to dehydroxylation, decomposition of calcite is considered irreversible and a presence of calcite in historical

ceramics is used as a marker for the firing temperature according to a rule „if the sample contains calcite, the firing temperature was below 800°C" [7].

The degree of conversion, which characterizes phase transformation of phyllosilicate or calcite during firing, depends on the temperature and time, $\alpha = f(T, t)$, if measured on small powder sample. A different situation is in a large ceramic body such as a brick. Layers which are on the surface are transformed sooner than the layers inside the brick. Experiments on large cylindrical samples (∅80 mm) showed clear dependence of the degree of kaolinite → metakaolinite conversion on the location of the small sample taken for TGA. Consequently, $\alpha = f(T, t, r)$, where r is the distance of the sample from the axis of rotation. It was also found that after heating at 650 °C for 10 h the degree of conversion reached ~0.95 and practically did not depend on r [9, 10].

In simple field kilns, which were used for firing bricks in the past, the fuel was beech wood [11]. Green bricks were prepared by molding the plastic mass made from local clay, silica sand or vegetal waste materials and water. Then the bricks were dried in a place protected again rain for several weeks and finally inserted into the kiln and fired. The firing process consisted from three steps. The first step was run at a low temperature to finish the removal of the physically bound water from pores. The second step was increasing the temperature up to the maximum determined by the technical capability of the kiln. As reported in [12, 13], the upper temperature limit in such a simple kiln is hardly higher than 700 °C–720 °C. The third step was slow cooling. The whole firing cycle took ~7 days in a small field kiln. We can assume that a similar method and equipment were used for firing the bricks of the Romanesque church in Pác sometime in the 13th century. The same we can assume for a Gothic period brickmaking because it did not significantly changed up to industrial revolution [14].

In this paper, the study is focused on the analysis of the bricks from the church in Pác. Our goal was to estimate the firing temperature.

2 Experimental

The samples were old pavement bricks from the church of St. Peter and Paul located in Pác, Trnava County, Slovakia. The church was originally built in the Romanesque style, was later rebuilt in the Gothic style in 15th century and enlarged in the Baroque style in 17th century. The pavement bricks come from the Romanesque and Gothic parts of the church. Romanesque pavement was later overlaid with Gothic pavement, overlaid with Baroque pavement. Both pavement bricks, Romanesque and Gothic, were directly in the open air for ~300 years.

The DTA and TGA were performed on the modernized Derivatograph 1000° (MOM, Hungary) [15] using compact samples of 10×10×20 mm cut from the bricks and a heating rate of 5 °C/min. A reference compact sample of the same size was made from a pressed powder Al_2O_3. The TDA was done on the dilatometer described in [16] with the sample 10×10×40 mm at the heating rate 5 °C/min.

The phase analysis was performed using the Powder X-ray diffraction on the diffractometer BRUKER D8 Advance under following conditions: Bragg-Brentano geometry (Theta-2Theta), Cu anticathode ($\lambda\alpha_1$ = 1.54060 Å), accelerating voltage 40 kV, beam current 40 mA. Ni Kβ filters was used for stripping of Kβ radiation on the primary and diffracted beam, and data was obtained by the BRUKER LynxEye detector. The step size was 0.01° 2Θ, the step time was 1 s per one step, and the range of measurement was 2 – 65 ° 2Θ. Measured data were evaluated with DIFFRAC^{plus} EVA software package using ICDD PDF-4+ database and Rietveld refinement with DIFFRAC^{plus} TOPAS was used for verification of identified phases.

3. Results and discussion

The results of XRD analysis of the bricks are illustrated in Fig. 1. Here, reflections of the four minerals are seen. Feldspar does not change its structure at the firing temperatures lesser than 950 °C and quartz transforms its structure at 573 °C reversibly. Thus the feldspar and quartz reflections can be considered the same as for the green bricks. Calcite is also present in the bricks, which shows that the firing conditions were not sufficient for its full decomposition. XRD reflections of illite were also found which also confirms lower firing temperature. The XRD patterns for the Romanesque and Gothic bricks are almost identical except a relatively small difference in quantitative proportions of albite and orthoclase feldspars (ca. 5%; based on the Rietveld refinement results). We can state, that clay for both bricks was dug in the very close places and the firing technologies were very similar.

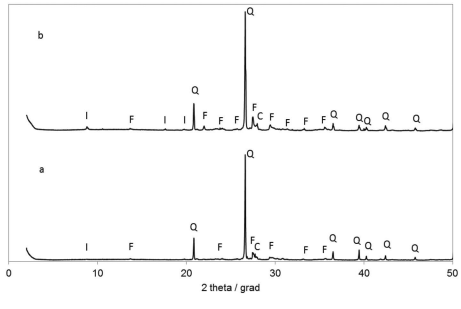

Fig. 1. XRD patterns of the Romanesque brick and Gothic brick. Q – quartz, F – feldspar, C – calcite, I – illite/muscovite
1. ábra Röntgendiffraktogramok (a) római kori tégla és (b) gótikus kori tégla. Q – kvarc, F – földpát, C – kalcit, I - illit, muszkovit

The results of DTA and TGA are illustrated in Fig. 2 and Fig. 3. The first endothermic minimum on the DTA curves, which belongs to the interval of 20 – 300 °C, is typical for porous building clay ceramics, which do not contain a glassy phase, i.e. fired at a relatively low temperature. The minimum is related to the liberation of the physically bound water absorbed on the surface of the mineral grains. It is known that the porosity of the green clay increases, for example porosity of the green porcelain mixture increases 4 – 5 % during dehydroxylation [17, 18]. In spite of the higher porosity, dehydroxylated ceramic body can absorb less water molecules than the green body. This can be explained by improved mechanical strength of the samples after dehydroxylation and less capability of the dehydroxylated samples to expand. This was observed on different green ceramic mixtures including illitic clay from a vicinity of the church [19].

The second step of the mass loss has sharp termination at ~840 °C which is a typical feature of the TGA curve of calcite decomposition [20]. Between these two significant mass losses, a gradual mass loss is present which can be explained by the presence of the dissociated water molecules, i.e. ions H^+ and OH^- on the crystal surfaces. To liberate such water, higher temperature (up to 600 °C) is necessary [21]. The second reason can be the liberation of OH^- which could insert itself into dehydroxylated clay during rehydroxylation. For

example, a measurable rehydroxylation was registered in 19th century bricks [8]. Neither the endothermic minimum on the DTA curve (Fig. 2) nor a clear step of mass loss on the TGA curve (Fig. 3), which could be ascribed to the intensive second dehydroxylation, were registered with these analyses. Rehydroxylation is very slow process [8] and ~300 years, when the bricks were in the open air, was probably not sufficiently long time for the binding of greater amount of OH^- into dehydroxylated clay structure. After that period, the new plaster and pavement were laid onto the bricks, therefore the bricks were protected from atmospheric moisture up to now.

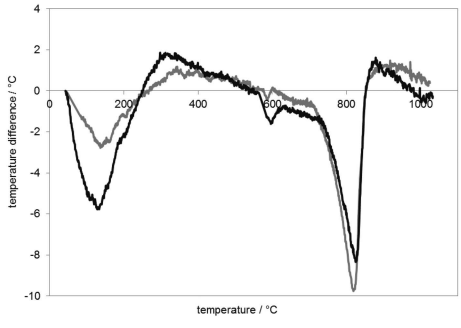

Fig. 2. Differential thermal analysis of the Gothic (gray) and Romanesque brick (black)
2. ábra Római kori tégla (fekete) és gótikus kori tégla (szürke) DTA görbéi

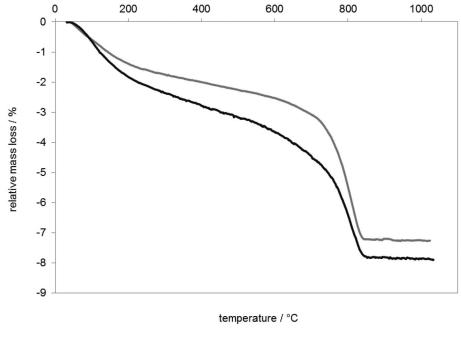

Fig. 3. Thermogravimetry of the Gothic (gray) and Romanesque brick (black)
3. ábra Római kori tégla (fekete) és gótikus kori tégla (szürke) TG görbéi

The results of TDA are visualized in Fig. 4. The TDA of the both bricks showed the presence of significant amount of quartz, which corresponds with a small DTA endothermic peak at ~570 °C. Above 700 °C, the TDA curves of the brick material begin to bend downwards, i.e. contraction of the sample takes place. It can be ascribed to decomposition of calcite [22]. After completion of this decomposition, the samples continue to expand up to the maximum experimental temperature 1000 °C. If the glassy phase is present in the bricks, it would be indicated on both TDA curves via typical contraction caused by the pressing force of the dilatometer's push-rod [23]. This contraction appears above transformation temperature of the glassy phase. Since the glassy phase can arise during firing at the temperatures higher than ~800 °C [4], we can state, that the maximum firing temperature of the both bricks was lower than 800 °C.

Both TDA curves depicted in Fig. 4 can be used for estimation of the firing temperature [4, 24, 25]. The thermal expansion method is based on the fact that when the partially fired clay body is subjected to a linear heating during TDA, shrinkage occurs above a certain temperature. The point on the dilatometric curve where contraction starts is considered the original firing temperature. According to this rule, the temperature ~720 °C, which corresponds to the beginning of the contraction, is the firing temperature for the both bricks. This contraction is caused by the decomposition of calcite which is accompanied with significant shrinkage [22, 23].

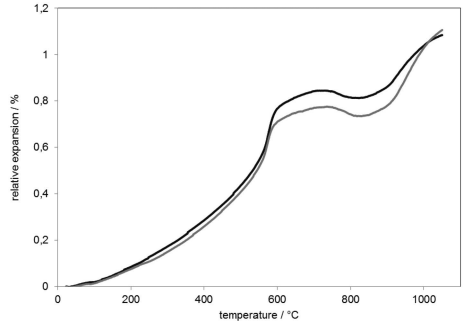

Fig. 4. Thermodilatometry of the Gothic (gray) and Romanesque brick (black)
4. ábra Római kori tégla (fekete) és gótikus kori tégla (szürke) termodilatometriai görbéi

If we suppose a firing schedule according to Fig. 5, we see that a period with temperatures higher than 450 °C, which are suitable for dehydroxylation, is~60 h long for 7-day firing. The period at 700 °C, where dehydroxylation runs very intensively, is also sufficiently long: ~35 h. In a case of the shorter isothermal heating, we have a period of 48 h with temperatures above 450 °C. That are sufficient times for completing dehydroxylation in a large body such as a brick.

As written above, the estimation of the firing temperature is based on the evaluation of the degree of transformation. Irreversible phase transformations, which we took into account, were dehydroxylation of phyllosicates and decomposition of calcite. A formation of a glassy phase is beyond the capability of the simple medieval kiln (heated with wood) which was supposedly used for the firing of bricks. Vitrification temperature of clays is higher than 700 °C, mostly above 800 °C [4]. As mentioned above, the degree of conversion depends on the temperature and time, i.e. the same degree of conversion we can obtain with lower temperature (which is from an interval of the relevant transformation) and longer time or with higher temperature and shorter time. But an influence of the temperature is stronger than the influence of the firing duration. These conditions results in a leftover amount of the dehydroxylated phyllosicates and calcite after firing (i.e. the degree of conversion), and consequently, the results obtained by the used method (TGA, DTA, TDA and XRD). Therefore, if we want to estimate the firing temperature, we should know a firing schedule. If the firing at high temperatures takes sufficient time, these reactions can be completed in the whole brick's volume. After analysis of the possible firing schedule (Fig. 5), we can conclude that there was enough time to complete dehydroxylation in the whole brick's volume at temperatures higher than 600 °C during minimally 35 h. We can say that the minimum firing temperature was ~600 °C. On the other side, the firing conditions were not sufficient for the total decomposition of calcite. The upper limit of the firing temperature can not be estimated from the decomposition of calcite only which expresses itself in Figs. 2 and 3 by the mass loss and endothermic minimum and by a contraction in Fig. 4.

Besides that, we should take into consideration the technical limit of the kiln. It was probably not higher than 700 °C.

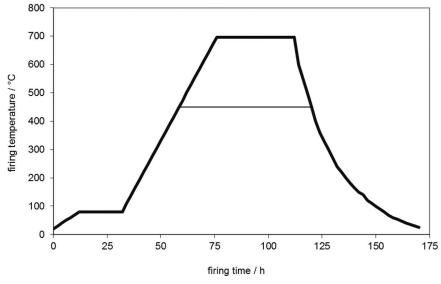

Fig. 5. The assumed firing schedule for 7-day firing with two different coolings
5. ábra Feltételezett égetési program a 7 napos égetés során. A 450°C feletti hőmérséklet elégséges a vízvesztéshez

4. Conclusions

Pavement bricks taken from a Romanesque and Gothic parts of the church in Pác in the Trnava County, Slovakia were investigated by XRD and thermal analyses DTA, TGA and TDA. It was found that the bricks contained dehydroxylated illitic clay, calcite and quartz. As revealed, dehydroxylation was completely finished and no significant rehydroxylation was observed. Decomposition of calcite was also observed. The estimated firing temperature is between 650 °C and 700 °C.

Both bricks were made from the local clay pits and very similar technologies were used in spite of the ~300 year time interval between their productions.

Acknowledgements

This work was supported by the grant VEGA 1/0646/12, Ministry of Education of Slovakia. One author (I.Š.) is indebted to prof. V.A. Drebuschchak (Novosibirsk State University, Russia) for his interest in our work and valuable comments.

References

[1] Kristály, F. – Kelemen, É. – Rózsa, P. – Nyilas, I. – Papp, I.: *Mineralogical investigations of medieval brick samples from Békés county (SE Hungary).* Archaeometry, 54 (2012) 250-266, http://dx.doi.org/10.1111/j.1475-4754.2011.00628.x

[2] Podolinský, Š.: *Cultural beauties of Slovakia, Romanesque churches.* Dajama, Bratislava 2009 (in Slovakian)

[3] Vandiver, P.: *The role of materials research in ceramics and archeology.* Annual Review of Materials Research, 31, (2001) 373-385 http://dx.doi.org/10.1146/annurev.matsci.31.1.373

[4] Tite, M.S.: *Determination of the firing temperature of ancient ceramics by measurement of thermal expansion: a reassessment.* Archaeometry, 11 (1969) 131-143, http://dx.doi.org/10.1111/j.1475-4754.1969.tb00636.x

[5] Drebuschchak, V.A. – Mylnikova, L.N. – Drebuschchak, T.N.: *The mass-loss diagram for the ancient ceramics.* J. Thermal Analysis and Calorimetry, 104 (2011) 459-466, http://dx.doi.org/10.1007/s10973-010-1230-x

[6] Drebuschchak, V.A. – Mylnikova, L.N. – Molodin, V.I.: *Thermogravimetric investigation of ancient ceramics.* J. Thermal Analysis and Calorimetry, 90 (2007) 73-79, http://dx.doi.org/10.1007/s10973-007-8478-9

[7] Drebuschchak, V.A. – Mylnikova, L.N. – Drebuschchak, T.N. – Boldyrev, V.V.: *The investigation of ancient pottery - Application of thermal analysis.* J. Thermal Analysis and Calorimetry , 82 (2005) 617-626, http://dx.doi.org/10.1007/s10973-005-6913-3

[8] Hamilton, A. – Hall, C.: *A review of rehydroxylation in fired-clay ceramics.* J. American Ceramic Society, 95 (2012) 2673-2678, http://dx.doi.org/10.1111/j.1551-2916.2012.05298.x

[9] Ondruška, J. – Trník, A. – Vozár, L.: *Degree of conversion of dehydroxylation in a large electroceramic body.* Int. J. Thermophysics, 32, (2011) 729-735, http://dx.doi.org/10.1007/s10765-010-0899-1

[10] Ondruška, J. – Trník, A. – Medveď, I.: *Estimation of mass transfer parameters during dehydroxylation in a large ceramic body by inverse methods.* Ceramics International, 37, 2011, 3299-3305, http://dx.doi.org/10.1016/j.ceramint.2011.05.126

[11] Kováč, F.: *The firing of bricks in field kilns.* Dom techniky, Bratislava 1960 (in Slovakian)

[12] *Road map for cleaner brick production in India.* Research report, Greentech Knowledge Solution, New Delhi, India, 2012

[13] *A study of a brick-making process along the Texas portion of the U.S.-Mexico border: Senate bill 749.* Report, Texas Commission on Environmental Quality, Austin 2002

[14] Laefer, D.F. – Boggs, J. – Cooper, N.: *Engineering properties of historic brick – variability considerations as a function of stationary versus nonstationary kiln type.* Journal of the American Institute of Conservation of Historic and Artistic Works, 4 (2004) 255-272

[15] Podoba, R. – Trník, A. – Podobník, Ľ.: *The upgrating of TGA/DTA analyzer Derivatograph.* Epitoanyag – Journal of Silicate Based and Composite Materials, 64 (2012) 28-29

[16] Štubňa, I. – Vážanová, A. – Varga, G. – Hrubý, D.: *Simple push-rod dilatometer for dilatometry of ceramics.* In: Proc. Conf. Research and Teaching of Physics, SPU Nitra, Nitra 2007, 69-74

[17] Štubňa, I. - Kozík, T.: *Permeability of the electroceramics to gas and its dependence on the firing temperature.* Ceramics International, 23 (1997) 247-249, http://dx.doi.org/10.1016/S0272-8842(96)00034-X

[18] Plešingerová, B. – Súčik, G. – Fabián, M.: *Surface area change of kaolin causing annealing.* Acta Metallurgica Slovaca, 17 (2011) 169-176

[19] Podobník, Ľ. – Jankula M. – Štubňa, I.: *Influence of dehydroxylation on hydration of illitic and kaolinitic clays.* XXV DIDMATTECH 2012, Book of Abstracts, JSU Komárno, 2012, 20-21

[20] Teleki, A. – Vozár, L. – Tóth, A.: *Kinetics of the irreversible chemical process.* In: Cophys – International Physics Workshop, UKF Nitra, Nitra 2008, 99-107 (in Slovakian)

[21] Kiselev, I.M.: *Firing of kaolin and investigation of fired products.* PhD thesis stored in ONIITECHIM, Čerkassy, 1978, No. 1762178 (in Russian)

[22] Tóth, A.: *Physical properties of lime before and after firing.* PhD thesis, UKF Nitra, Nitra 2009 (in Slovakian)

[23] Ventureli, C. – Paganelli, M.: *Sintering behavior of clays for the production of ceramics.* Cfi/Ber. DKG, 84, (2007) N5, E1-E3

[24] Roberts, J.P.: *Determination of the firing temperature of ancient ceramics by measurement of thermal expansion.* Archaeometry, 6 (1963) 21-23, http://dx.doi.org/10.1111/j.1475-4754.1963.tb00574.x

[25] Petrovič S. – Jovanov, V. – Vujovič, S. – Ranogajec. J.: *Historical materials from the medieval fortress Bač.* Processing and Application of Ceramics, 1 (2007) 75-80, http://dx.doi.org/10.2298/PAC0702075P

Ref.:
Igor **Štubňa** – Rudolf **Podoba** – Peter **Bačík** – Ľuboš **Podobník**: *Romanesque and Gothic bricks from church in Pác – estimation of the firing temperature*
Építőanyag, 65. évf. 2. szám (2013), 48–51. p.
http://dx.doi.org/10.14382/epitoanyag-jsbcm.2013.11

Római és gótikus kori téglák Pác templomából – Az égetési hőmérséklet becslése

Pác (Trnava megye, Szlovákia) templomának anyagából vett római kori és gótikus kori tégla mintákon végeztünk röntgendiffrakciós (XRD) és termoanalitikai (DTA, TGA, TDA) vizsgálatokat. A vizsgálatok a téglák anyagában kristályvízmentes illit agyagásványt, kalcitot, kvarcot és földpátot mutattak ki. Bebizonyosodott, hogy az illit vízvesztése teljes mértékben lejátszódott, és utólagos kristályvíz beépülés nem volt kimutatható. Az égetési hőmérséklet becsült értéke 650°C és 700°C közé tehető. Mindkét tégla helyi agyag felhasználásával készült nagyon hasonló technológiával.
Kulcsszavak: történeti kerámiák, termikus vizsgálat, égetési körülmények

Simple basic model for concrete and its application

1. Content indicators of concrete mixtures and mixing plant observations

Gyula PEKÁR ▪ private consultant ▪ alba-qualit@hdsnet.hu

Érkezett: 2013. 06. 06. ▪ Received: 06. 06. 2013. ▪ http://dx.doi.org/10.14382/epitoanyag-jsbcm.2013.12

Abstract

One of the constantly recurring tasks of concrete engineering is to examine the effects and interactions of the materials which concrete mixtures are composed of. When analysing the effects and interpreting the interactions, it is often worth going back to the basics and reconsidering the models that we use to interpret our findings. It may be necessary to refine them, so that the models we use as the basis for concrete mix design keep pace with the developments brought about by the appearance of new materials. The paper introduces a simple basic model for concrete mixtures that covers dimensionless content indicators which can determine the composition of concrete in a clear and predictable way. The content indicators have an impact on the performance properties of the concrete, therefore, specific direct observations were made and measurements were carried out at a concrete mixing plant. The observations provided data input for the simple basic model for concrete mixes, which, by introducing dimensionless concrete composition content indicators, offers a new way of examining the effects that influence the performance properties of fresh and hardened concrete mixes.

Keywords: concrete technology, concrete mix design, concrete composition content indicators

Gyula PEKÁR

Chemical engineer (University of Veszprém, 1981). Active in the construction industry since 1984, first as a research engineer, and later as head of the laboratory at ARÉV, which was at the time the leading construction company in Székesfehérvár. From 2000, as a private consultant, he prepared enterprises for the implementation and operation of a number of QA systems (ISO 9001, ISO 14001, ISO/IEC 17025). From 2007-2013 he was a part-time engineering inspector at the state-owned ÉMI (Non-Profit Limited Liability Company for Quality Control and Innovation in Building). With the support of ÉMI, he carried out a research project, originally in conjunction with the Augusztin Concrete Manufacturing Company (Zamárdi), to establish the correlations between concrete compositions and the performance indicators of the set concrete, by recording observations of concrete mixes during their manufacture at the mixing plant. In 2011, he was invited by the Hungarian Institute for Transport Sciences to participate in research into low-shrinkage floor concrete compositions.

1. Introduction

There are certain phenomena sometimes in concrete technology which do not fit in the existing models (or do not fit in very easily), as can be illustrated by the following three examples on the effects of *cements*, *additions* (supplementary materials) and *water-reducing admixtures*.

In the *Hungarian Concrete Almanac 2005, Szalai*, *Huszár* and *Sprániz* indicated that in *cases of low water-cement ratios (w/c<0.4) a greater compressive strength can be measured for certain CEM 32.5 cements than for CEM I 42.5 and CEM I 52.5 cements*, which seems to contradict the widely known equations for estimating compressive strength [1]. Own tests of the authors of present paper confirm this: in the case of mixtures where w/c=0.2, it was found that specimens made of CEM III/B 32.5 N-S type cement after a period of 28 days had higher compressive strength (136.7 N/mm^2) than that of the mixture made with CEM I 42.5 cement and cured under identical conditions (129.8 N/mm^2). *Could there possibly be a method of estimating compressive strength which is able to predict these apparently contradictory results?*

Zsigovics – the first researcher in Hungary who studied the effects of *additions* on concrete mixes – reported another interesting observation: a series of concrete mixes was prepared using identical dosage of cement (350 kg/m^3), identical water-cement ratio (w/c=0,5) and identical quantity of water-reducing admixture (1.6%), but with the content of limestone powder varying between 70 kg/m^3 and 370 kg/m^3. Increasing the amount of limestone powder to its upper limit has increased the compressive strength by 55%, while the consistency measured using flow table test has been increased by 20% [2]. *How can we explain this?*

Determining the consistency of concrete mixtures could be also difficult when effective *water-reducing admixtures* are used to achieve the required results. It is worth here taking a look at *Sulyok*'s reports considering two major investigations in Hungary: the Budapest Metro and the M6 Motorway [3,4]. *Sprániz* provides a very thorough survey of the discrepancies appearing in the effects of different admixtures and the combined effects of additions in cement pastes [5]. Research findings and practical experience both confirm that *the effect of water-reducing admixtures depends on the prevailing compositional (environmental) properties of the concrete mixtures.* In addition to the *type of admixture*, exactly when and to what extent the effect takes place depends, for example, on the *paste content* of the concrete, the water content of the paste and the grading (specific surface area) of the aggregate. *The question is "simply" what are the specific relationships that describe the consistency of fresh concrete mixtures with or without admixtures?*

Is it possible that the phenomena and problems referred to above are interrelated? They probably are, and they can ultimately be traced back to the *compositional and environmental properties (conditions)* of the concrete mixtures. If this really is the case, then *there must be a model based on the compositional properties of concrete*, into which we can fit the phenomena that are mostly dealt with today on a purely empirical basis. The present work is intended to present the basis of such a model.

2. A brief review of the paste approach in concrete technology

Both European standard EN 206-1 and Hungarian standard MSZ 4798-1:2004 (which is a National Application Document to EN 206-1) define concrete as *"…a material formed by mixing cement, coarse and fine aggregates and water, with or without the incorporation of admixtures or other additions…"* This listing of the constituent materials of concrete is almost too literal. It is also rather thought-provoking that this extensive standard

only mentions the word *paste* on very rare occasions (perhaps eight times in all). This is especially peculiar given the whole life work of *Powers* [6], as well as the fact that *Ujhelyi*, in his pioneering research on concrete engineering in Hungary, has not only used the concept of paste for decades, but has also carried out systematic studies of the effects of paste on the performance properties of concrete mixtures [7]. The *paste approach* was published in the technical directive MÉASZ ME 04-19:1995, again as a result of work by *Ujhelyi* and his colleagues [8], and it remains to this day a vital resource of information for all concrete engineers in Hungary.

The *paste approach* is therefore with us, even if it has not yet achieved the rank of being recognised in the standard, and it is used by engineers in the forefront of concrete research and practice. In an article published several years ago, *Sprán itz* wrote about the composition of concrete mixtures by stating the *volume ratios of paste content and air content*, including the *volume ratio of water and powder* (particles below 0.125 mm) in the paste, with the additions calculated together with the other powder materials [9]. The traditional water-cement ratio was also given in the paper, so that an expert can easily calculate the recipe from his data. However, the main issue here is not the recipe, but the approach. If we say that the concrete mixture contains *530 litres of paste per 1 m³* (x=0.56 water/fine particle volume ratio, w/c=0.24 traditional water-cement ratio), in which 70% (v/v) of the paste powder is cement, and also there is *10 litres of air* in the concrete (from which we get a volume of *460 litres of aggregates*), this reveals much more about the structure of the concrete than by listing the recipe like the ingredients in a cookery book. The same concrete composition can also be described as *c=792 kg/m³*, *mixture of additions=298 kg/m³*, *water + admixture =191 kg/m³*, *aggregate=1219 kg/m³*, but whereas the first description tells us immediately that we are dealing with a mixture very rich in paste which will need to be strongly plasticized (and which will produce certain side effects when it is poured into the form), the cookery book list tells us very little indeed, unless we can mentally work out the concrete composition components into a structure in our mind.

We should therefore *move on* from a definition of (and approach to) concrete which is based on a listing of the components, and, building on the experiences gained so far in the area of research into high performance concretes, we should apply a simple basic model which, although not entirely without precedent, still requires further work to clear up the details and to refine its form. This model can help *to identify* the effects on certain performance properties of fresh and hardened concretes, and *to better understand* certain interrelationships, as well as serving as the basis for designing concrete compositions.

3. The simple basic model of concrete mixtures

Below we will consider the fresh concrete mixture as a macro-heterogeneous system which - at least from a macroscopic aspect - consists of three clearly distinct *phases*:

- *paste*, which is in itself a heterogeneous system (*micro-heterogeneous suspension)*, and which behaves in fresh concrete mixtures as a quasi-fluid *dispersing agent*,
- *aggregates*, which are a mass of *solid* (insoluble) macro-sized particles/granules, and which are distributed in the paste as a *dispersed phase*,
- *air*, as gaseous phase, which is generally present as *voids* as a result of incomplete compaction, although there are also conscious engineering processes whereby small air bubbles are introduced *intentionally* into the system (the paste) as a *dispersed phase*.

The composition of a given concrete mixture – for given paste and given aggregate (mixture) – is clearly given by *two independent data* – selected as appropriate – as per Eq. (1):

$$p + a + l = 1 \qquad \textbf{(1)}$$

where *p*, *a*, *l* are the *volumetric proportions* of *paste* (*p*), *aggregate* (*a*) and *air* (*l*) in the concrete, and where the aggregate may also be a *mixture* of a number of components $n_{AG} \geq 1$, with the restriction on the amount of the dose, Eq. (2):

$$a = \sum_{i=1}^{nAG} a_i = 1 - l - p \leq a_{\max} \qquad \textbf{(2)}$$

where a_{max} is the maximum volume ratio of aggregate that can be compacted into the volumetric unit of the concrete in the given compositional condition (equivalent to the amount designated by *Ujhelyi* as V_{a0} in [8], but expressed here as a dimensionless proportional figure), and a_i is the *i*-th volume ratio of the aggregate component in the component.

If the known or recorded α_{AGi} *volumetric proportions* of the aggregate are given, any a_i component can be expressed, Eq. (3):

$$a_i = \alpha_{AGi} \cdot a, \quad \text{where} \quad \sum_{i=1}^{nAG} \alpha_{AGi} = 1 \qquad (3)$$

If instead of the α_{AGi} *volumetric proportion* we insist on using the widespread $\alpha_{M,AGi}$ *mass proportions*, then the figure for volumetric proportion in Eq. (3) may be replaced by Eq. (4):

$$\alpha_{AGi} = \frac{\frac{\alpha_{M,AGi}}{\rho_{AGi}}}{\sum_{i=1}^{nAG} \frac{\alpha_{M,AGi}}{\rho_{AGi}}}, \text{ where } \sum_{i=1}^{nAG} \alpha_{M,AGi} = 1 \qquad \textbf{(4)}$$

where ρ_{AGi} is the particle density of the *i*-th aggregate in its condition when it is included in the mixture (in practice there are differences in the densities of different aggregate fractions and types, also depending on the amount of absorbed water, and these must be accounted for in the design).

4. The role of paste in the simple basic model for concrete mixtures and relationships

In the simple basic model for concrete mixtures, paste is considered (on the basis of its *macroscopic* properties and effects) as a phase of the concrete mixture that behaves as a quasi-fluid, in which (as it is itself a suspension) we can distinguish between different phases:

- the *fluid* phase (i.e. a mixture of *water + admixtures;* solution), which is the *dispersing agent* of the solid paste powder, and

- the *solid* phase (i.e. the paste powder), which is dispersed in the fluid as a *dispersed phase* as a mixture of the *fine particle content* of the *cement* + *additions* + aggregates, and also
- the *gaseous* phase (air), which may be present both as *entrapped* and or *entrained air* as a dispersed phase (and is present in practice).

We should clarify, when referring to the paste powder, that the *paste powder* includes the total of all *solid* state concrete components which have a particle size below a given limit (0.063 mm), regardless of whether they have hydraulic properties or not, or whether they have been intentionally measured into the mixture or have just added to the fresh concrete mixture, for example as a part of the aggregate. The limit for particle size (0.063 mm) is arbitrary, although this has no effect on the principle of the simple basic model (the difference between the *paste powder* and the *aggregate* appears not so much in the particle size as in the difference of *two* magnitudes between their *specific surface areas*).

It is worth stating some of the basic relationships regarding the composition of pastes. The *volumetric* composition of a paste of a given quantity is given by Eq. (5):

$$p = f + z = z \cdot (1 + x), \text{ where } x = \frac{f}{z} \quad (5)$$

where f and z are respectively the unabsorbed (free) *fluid* (mostly water) and the *volume proportion of the paste powder* in the concrete, and x is the *volumetric ratio* between the fluid and the paste powder, which functions are similar to the traditional water-cement ratio.

In addition to *cement* the paste powder may contain a $n_K \geq 0$ quantity of *addition components* as per Eqs. (6) to (7):

$$z = \frac{p}{1+x} = c + \sum_{i=1}^{nK} k_i = c + k \quad (6)$$

$$k_i = \alpha_{Ki} \cdot k, \text{ where } \sum_{i=1}^{nK} \alpha_{Ki} = 1 \quad (7)$$

where c, k_i, and k, are respectively the *volumetric ratios* of *cement*, the i-th *addition component* and the *total additions* in the concrete, and α_{Ki} is the volumetric ratio of the i-th component in the additions. If, instead of the volumetric ratio α_{Ki} we would rather use the *mass ratio* $\alpha_{M,Ki}$, then (taking the particle density ρ_{Ki} of the *additions* into account) we must recalculate according to Eq. (4) and use this in Eq. (7) in the place of α_{Ki}.

In addition to *water* the fluid phase of the paste may contain a $m \geq 0$ quantity of *admixture components*, as a perfect analogy of Eq. (6), see Eq. (8):

$$f = \frac{p}{1+x} \cdot x = w + \sum_{i=1}^{m} ad_i = w + ad \quad (8)$$

where w, ad_i and ad are respectively the *volumetric ratios* of unabsorbed *water*, the i-th *admixture component* and the *total admixtures* in the concrete.

If the quantity of the i-th admixture is expressed as the proportion λ_{ADi} of the volume of *paste powder*, then Eqs. (9) and (10) can be formulated:

$$\lambda_{ADi} = \frac{ad_i}{z} \quad (9)$$

$$ad = \sum_{i=1}^{m} ad_i = z \cdot \sum_{i=1}^{m} \lambda_{ADi} = \frac{p}{1+x} \cdot \sum_{i=1}^{m} \lambda_{ADi} \quad (10)$$

In order to verify the composition criteria according to Hungarian standard MSZ 4798-1:2004, it is important to take into consideration the combined volumes of water in the admixtures when calculating the water-cement ratio, which can be done by Eq. (11):

$$w_{AD} = \sum_{i=1}^{m} \frac{ad_i \cdot \rho_{ADi} \cdot (1 - sz_i)}{\rho_w} = \frac{p}{1+x} \cdot \sum_{i=1}^{m} \frac{\lambda_{ADi} \cdot \rho_{ADi} \cdot (1 - sz_i)}{\rho_w} \quad (11)$$

where w_{AD} is the amount of water in the admixture as a proportion of the volume of the concrete, ρ_{ADi} and ρ_w are respectively the *density* of the *admixture* and the *water* in the given environmental condition, and sz_i is the *dry matter content* of the i-th admixture expressed as a mass ratio (manufacturers usually provide the information as a percentage of mass).

Finally, proportional parameters can be introduced for paste powder components, Eq. (12):

$$\beta_k = \frac{k}{c}, \text{ or rather } \chi_c = \frac{c}{z} = \frac{1}{1+\beta_k} \quad (12)$$

where β_k and χ_c are respectively the *volumetric ratios* of *additions/cement* and of *cement/paste powder*.

5. Content indicators used in the simple basic model for concrete mixtures

If a concrete mixture *does not contain* admixtures or additions, so $\chi_c = 1$ [i.e. $\beta_k = 0$] and $\lambda_{ad} = 0$, then the ratios p (volumetric ratio of paste in the concrete), x (liquid-powder volumetric ratio in the paste) and l (volumetric ratio of air in the concrete) – *in the case of given concrete component materials* – clearly determine the composition of the concrete.

If a concrete mixture also contains *additions* and/or *admixtures*, then in order to be able to clearly determine the composition of the concrete we also need to know two additional ratios: χ_c (proportion of cement in the paste powder) and λ_{AD} (the sum of all λ_{ADi}-s, the combined volume ratio of all admixtures compared with the *paste powder*). Instead of χ_c we may opt to use the proportional figure β_k (the sum of all β_{ki}-s, the combined volume ratio of all additions compared with the cement), as they can both be derived from each other using Eq. (12).

In the case of *fixed* α_{Ki}, λ_{ADi} and α_{AGi} composition proportions of multi-component concrete constituents (additions, admixtures and aggregates), the five dimensionless ratios (p, x, l, χ_c λ_{AD}) are necessary and sufficient to describe the composition of concrete mixtures, and therefore these ratios may also be regarded as *concrete composition content indicators*. Later we will not only use these parameters to *describe* (and compare) concrete

Structure	Constituents	content indicators, ratios					densities [kg/m³]	equations		composition [kg/m³]	composition [l/m³]
paste	Water, **w**	f	$p = f+z = 0{,}348$	$x = f/z = 1{,}074$			**1000**	(13) W [kg/m³] =	$\frac{p}{1+x}\cdot\left(x\cdot\rho_w - \sum_{i=1}^{m}\lambda_{ADi}\cdot\rho_{ADi}\right)\cdot V_b$	**175**	***175***
	admixture, **ad**				$\lambda_{AD}=ad/z$	**0,030**	**1100**	(14) ADi [kg/m³] =	$\lambda_{ADi}\cdot\frac{p}{1+x}\cdot\rho_{ADi}\cdot V_b$	**5,54**	***5,03***
	cement, **c**	z			$\chi_c=c/z$	***0,681***	**3065**	(15) C [kg/m³] =	$\chi_c\cdot\frac{p}{1+x}\cdot\rho_c\cdot V_b$	**350**	***114***
	additions, **k**				$\beta_k=k/c$	*0,468*	**2710**	(16) Ki [kg/m³] =	$\alpha_{ki}\cdot(1-\chi_c)\cdot\frac{p}{1+x}\cdot\rho_{Ki}\cdot V_b$	**145**	***54***
aggregates	0/4, **a1**	$a = 1-l-p = 0{,}631$			α_{AG1}	**0,50**	**2640**	(17) AGi [kg/m³] =	$\alpha_{AGi}\cdot(1-p-l)\cdot\rho_{AGi}\cdot V$	**833**	***316***
	4/8, **a2**				α_{AG2}	**0,35**	**2640**			**583**	***221***
	8/16, **a3**				α_{AG3}	**0,15**	**2640**			**250**	***95***
air (void)	***l***	***l=0,021***					**1,29**	L [kg/m³] =	$l\cdot\rho_{lev}\cdot V_b$	**0**	***21***

Table 1. Composition of concrete with content indicators p=0.348, x=1.074, l=0.021, λ_{ad}=0.030, χ_c=0.681 from concrete components
1. táblázat Egy p=0.348, x=1.074, l=0.021, λ_{ad}=0.030, χ_c=0.681 állapotjelzőjű beton összeállítása a betonalkotókból

compositions; we will also examine the relationships between the *content indicators* and certain *performance properties* of fresh and hardened concretes. Of course, the performance properties of concretes are not exclusively influenced by the concrete composition content indicators, but also by the actual *physical properties* of the concrete constituents. The model based on concrete composition content indicators does, however, offer a basic framework for interpreting the properties of concretes, and supports a way of assessing the similarities of different concrete compositions (the five independent content indicators provide virtually infinite possibilities, so there is no need to worry that there will be no more areas in concrete engineering that require further research).

An example is presented as an illustration of a concrete mixture with given content indicators *p*, *x*, *l*, χ_c λ_{adi}, where the material properties of the concrete components are given. Calculations of a concrete composition with a volume of V_b=1 m³ from the content indicators are presented in *Table 1*, while the pie chart in *Fig. 1* shows the quantities C, K, W, AD_i, AG_i of *known* concrete components that are to be added to 1 m³ of concrete mixture.

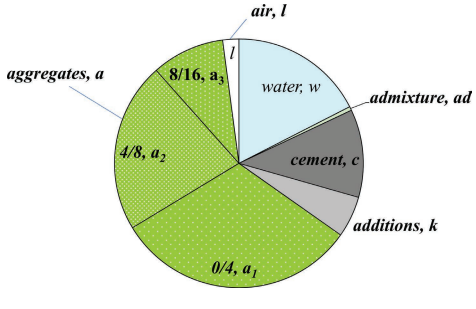

Fig. 1. Volumetric composition of concrete with content indicators p=0.348, x=1.074, l=0.021, λ_{AD}=0.030, χ_c=0.681
1. ábra A p=0,348, x=1,074, l=0,021, λ_{AD}=0,030, χ_c=0,681 állapotjelzőjű beton térfogatos összetétele

6. Observations at a concrete mixing plant

The author of present paper worked together with Augusztin Betongyártó Ltd. concrete mixing plant on various projects since 2007. The initial task was simply to conduct maintenance on the mixing recipes used at the concrete mixing plant of Augusztin Betongyártó Ltd., which was done mainly in line with the former Hungarian standard MSZ 4719:1982. The maintenance was needed due to changes that had taken place in the aggregates used at the mixing plant, but the possibility of changing the types of cement used and introducing certain additions was also raised. The original task was continued in *R+D cooperation* with new objectives under the support of ÉMI Nonprofit Ltd. from 2009.

Nevertheless, a series of observations at a mixing plant does not need much preparation to carry out, however, there is a need for organisation and discipline. When the aim is to collect a mass of data which can be used for proper analysis and for subsequent evaluations, it is important to extend the level of observation over the level of a regular mixing plant inspection.

7. Conditions of the observations

The conditions for carrying out the mixing plant observations were defined as early as 2008 as follows:

- The plant should be equipped with a *system of certified scales* for accurately weighing in the concrete constituents.
- For every batch of concrete mix that is subject to observation, the *dosage of every single constituent in the concrete must be known and recorded.* In the case of aggregate fractions, the measurement to be recorded is of the aggregate at the time of mixing, that is, the aggregate is *wet*. Even relatively small doses of admixtures must not be neglected. In view of the fact that individual deliveries of concrete are often composed of *more than one mixing item*, it is needed to include *summarised data* of the mixing items in the database of deliveries.
- Certain physical properties of the concrete constituent materials must be *continuously* known or monitored, *at least* the physical properties which are described in detail later in this paper.

- For every sample taken from the concrete mix deliveries *which are included in the observations*, at least the following tests and data must be recorded:
  - inspection of *consistency* of the sample within half hour of the start of the mixing process, with at least one measurement of consistency defined (such as flow table and/or slump),
  - concrete *temperature*, air *temperature*, air *humidity*, wind speed if necessary,
  - determination of the *water content* of the sample as the mass proportion or mass percentage of the fresh concrete ($w_{concrete}$),
  - at least three sample cubes with dimensions of 150 mm must be taken, and the *mass of the fresh concrete* compacted into the mould must be measured (the $\rho_{concrete}$ fresh particle densities can also be determined from this),
  - the *air content* of the samples must be inspected, which in theory directly tells us *content indicator l*, although it is always worth carrying out calculations of this to check that the particle densities and water contents of the samples confirm the result of the air-content inspection,
  - after removal from the mould after one day, specimens must be *submerged in water* until the 28th day (in spite of all views to the contrary, only wet, saturated $Ca(OH)_2$ solution storage provides curing conditions that may be regarded as identical),
  - the *dimensions* of the sample cubes must be measured after they are taken out from the moulds, or at the latest before the strength test,
  - *repeat* the measurement of the mass before the compressive strength test (compared with the *fresh concrete, the concrete which is kept submerged in water always absorb more water* [10], which could be a significant parameter typical of the type of cement),
  - *Compressive strength test* at a known age (in general at 28 days; as was in present analyses).

In addition to the tests listed above, additional inspections may also be carried out: these may include inspections of the *consistency endurance* and early-age and mature compressive strength at different ages and in different environmental conditions, the *splitting tensile strength* tests, the *deformation* properties, examination of *resistance to certain (material) transport processes*, etc. To conduct the tests it is necessary to have *properly trained staff* and *certified measuring instruments*, or if these are not available it is recommended to use the services of a properly equipped and, if possible, *accredited testing laboratory*.

In theory, the number of tests that can be carried out is infinite, but for the simple basic model one criterion is always essential: the concrete *composition content indicators* of the concretes being inspected must always be known or calculable, in addition to the physical and other material properties of the concrete constituents that must also be known. Here the question arises of how concrete composition content indicators are derived from the mixing plant observation data and the known or measured physical properties.

8. Defining concrete composition content indicators from observed data

Before the definition of the concrete composition content indicators, list of observed data available for calculating the content indicators is given.

8.1 Dosage (weighed) quantities

K_{virt} (kg) total measured additions, c (kg) measured cement, AG_{virt} (kg) total measured wet aggregates, W_{virt} (kg) measured added water, AD (kg) total measured admixtures. The *virt* (virtual, apparent) index in the quantities refers to the fact that there are (or may be) parts present in the concrete constituents, which belong to different phase components of the concrete. For example, in the case of the *additions*, besides the parts that belong to the *paste powder* phase there are also particles above 0.063 mm, which belong to the *aggregate* phase, while there are at the same time particles in the aggregate below 0.063 mm, which belong to the paste powder. Moreover, in the aggregates there is also water present, which must be accounted for in addition to the water which is added when the batch is mixed.

The dosage (weighed) results clearly provide the dosage *mass ratios* ($\alpha_{M,Kvirt,i}$, $\alpha_{M,AGvirt,j}$, $\alpha_{M,AD,k}$) for each type of concrete constituent, where the sum of the ratios is unity as: $\Sigma\alpha_{M,Kvirt,i} = \Sigma\,\alpha_{M,AGvirt,j} = \Sigma\,\alpha_{M,AD,k} = 1$.

8.2 Physical properties of the concrete constituents

- The *moisture contents* of the aggregate fractions ($w_{AG,,j}$; m%) in the condition they are in when mixed into the concrete.
- The *fine particle* (<0.063 mm) contents of the additions and the aggregate fractions as a mass proportion ($\phi_{K,i}$, $\phi_{AG,j}$; m%).
- The *particle densities* of the aggregate fractions (kg/m^3), at the very minimum for *fine* (<0.063 mm) and *coarse* (>0.063 mm) particles ($\rho_{AG,coarse,j}$, $\rho_{AG,fine,j}$).
- The *relative densities* of the *cement*, the *additions*, the *mixing water* and the *admixtures* (ρ_c, $\rho_{K,i}$, ρ_w, $\rho_{AD,k}$; kg/m^3) in their condition at the time of mixing.
  For cements and additions the calculations are made using their dry densities, while for aggregates it is sensible to use the *surface-dry, water-saturated* density.
- It is a good idea to collect data on the *short-term water absorption rates* of the solid concrete constituents (cement, additions and aggregates) (sw_c, $sw_{K,i}$, $sw_{AG,j}$; m%), because their impact may be discernible in the case of concretes with a low water-cement ratio. When processing and evaluating the data from the observations at the mixing plant within the spectrum of conventional concretes, we generally did not account for this impact.
- The *dry matter contents* of admixtures (sz_i; m%).

$$V_{b,\,compacted} = \mathbf{K}_{virt} \cdot \sum_{i=1}^{nK} \alpha_{M,\,Kvirt,\,i} \cdot \left(\frac{1}{\rho_{K,\,i}} - \frac{SWK,\,i}{\rho_w} \right) + \mathbf{c} \cdot \left(\frac{1}{\rho_c} - \frac{SWc}{\rho_w} \right) + \mathbf{AG}_{virt} \cdot \sum_{j=1}^{nAG} \frac{\alpha_{M,\,AGvirt,\,j}}{1 + w_{AG,\,j}} \cdot \left(\frac{1 - \varphi_{AG,\,j}}{\rho_{AG,\,coarse,\,j}} + \frac{\varphi_{AG,\,j}}{\rho_{AG,\,fine,\,j}} + \frac{W_{AG,\,j} - SWAG,\,j}{\rho_w} \right) + \frac{\mathbf{W}_{virt} - \Delta\mathbf{W}_{ev}}{\rho_w} + \mathbf{AD} \cdot \sum_{k=1}^{nAD} \frac{\alpha_{M,\,AD,\,k}}{\rho_{AD,\,k}} \quad (18)$$

$$V_b = \frac{V_{b,\,compacted}}{1 - l} \quad (19)$$

$$z = \frac{\mathbf{K}_{virt} \cdot \sum_{i=1}^{nK} \alpha_{M,\,Kvirt,\,i} \cdot \frac{\varphi_{K,\,i}}{\rho_{K,\,i}} + \frac{\mathbf{c}}{\rho_c} + \mathbf{AG}_{virt} \cdot \sum_{j=1}^{nAG} \frac{\alpha_{M,\,AGvirt,\,j}}{1 + w_{AG,\,j}} \cdot \frac{\varphi_{AG,\,j}}{\rho_{AG,\,fine,\,j}} + \mathbf{AD} \cdot \sum_{k=1}^{nAD} \alpha_{M,\,AD,\,k} \cdot \left(\frac{1}{\rho_{AD,\,k}} - \frac{1 - SZk}{\rho_w} \right)}{V_{beton}} \quad (20)$$

$$f = \frac{-\mathbf{K}_{virt} \cdot \frac{\sum_{i=1}^{nK} \alpha_{M,\,Kvirt,\,i} \cdot SWK,\,i}{\rho_w} - \mathbf{c} \cdot \frac{SWc}{\rho_w} + \mathbf{AG}_{virt} \cdot \sum_{j=1}^{nAG} \frac{\alpha_{M,\,AGvirt,\,j}}{1 + w_{AG,\,j}} \cdot \frac{W_{AG,\,j} - SWAG,\,j}{\rho_w} + \frac{\mathbf{W}_{virt} - \Delta\mathbf{W}_{ev}}{\rho_w} + \mathbf{AD} \cdot \sum_{k=1}^{nAD} \alpha_{M,\,AD,\,k} \cdot \frac{1 - SZk}{\rho_w}}{V_{beton}} \quad (21)$$

$$x = \frac{f}{z} \quad (22)$$

$$p = f + z \quad (23)$$

$$\chi_c = \frac{\mathbf{c}}{z} \cdot \frac{1}{\rho_c} \cdot \frac{1}{V_{beton}} \quad (24)$$

$$\sum_{k=1}^{nAD} \lambda_{AD,\,k} = \frac{ad}{z} = \frac{\mathbf{AD} \cdot \sum_{k=1}^{nAD} \frac{\alpha_{M,\,AD,\,k}}{\rho_{AD,\,k}}}{z} \cdot \frac{1}{V_{beton}} \quad (25)$$

$$\frac{\mathbf{v}}{\mathbf{c}} = \frac{-\mathbf{K}_{virt} \cdot \sum_{i=1}^{nK} \alpha_{M,\,Kvirt,\,i} \cdot SWK,\,i + \mathbf{AG}_{virt} \cdot \sum_{j=1}^{nAG} \frac{\alpha_{M,\,AGvirt,\,j}}{1 + w_{AG,\,j}} \cdot \left(w_{AG,\,j} - SWK,\,i \right) + \mathbf{W}_{virt} - \Delta\mathbf{W}_{ev} + \mathbf{AD} \cdot \sum_{k=1}^{nAD} \alpha_{M,\,AD,\,k} \cdot \left(1 - SZk \right)}{\mathbf{c}} \quad (26)$$

Table 2. Equations for calculating concrete composition content indicators from the dosages of concrete constituents and data on their physical properties
2. táblázat A betonösszetételi állapotjelzők számítási képletei a betonalkotók adagolási mennyiségeiből és fizikai jellemzőinek adataiból

8.3 Measurements used for calculating the concrete composition content indicators

- The measured masses (kg) of the components of the fresh concrete batch, in line with the first paragraph of section 8.1.
- In periods of hot weather it is sensible to measure, estimate and *account for* the *loss through evaporation* ΔW_{ev} (kg) experienced by the mixed items.
- The measured air content of the fresh concrete, *l* as a volume ratio of the concrete (directly measured content indicator).

8.4 Measurements used both for calculating the concrete composition content indicators and for checking the calculations

- *Particle density* as measured in the fresh concrete $\rho_{concrete}$ (kg/m^3).
- *Water content* as measured in the fresh concrete $w_{concrete}$ (m%).

8.5 Calculating the concrete composition content indicators

The auxiliary variables used in the calculations can be derived by Eqs. (18) to (21); the four concrete composition content indicators (apart from *l*) and the traditional (effective) water-cement ratio can be derived using equations (22) to (26). The interrelationships – without detailed calculations – are presented in *Table 2*.

When defining the concrete composition content indicators it is important also to check if the *measured values* (i.e.: *measured density*, $\rho_{concrete}$, kg/m^3 and *measured water content* $w_{concrete}$, m%) of the fresh concrete match the values *calculated* using Eqs. (27) and (28) below:

$$\rho_{concrete,\,calc} = \frac{\mathbf{K}_{virt} + \mathbf{c} + \mathbf{AG}_{virt} + \mathbf{W}_{virt} - \Delta\mathbf{W}_{ev} + \mathbf{AD}}{V_c} \quad (27)$$

$$W_{concrete,\,calc} = \frac{\mathbf{AG}_{virt} \cdot \sum_{j=1}^{nAG} \frac{\alpha_{M,\,AGvirt,\,j}}{1 + w_{AG,\,j}} \cdot w_{AG,\,j} + \mathbf{W}_{virt} - \Delta\mathbf{W}_{ev} + \mathbf{AD} \cdot \sum_{k=1}^{nAD} \alpha_{M,\,AD,\,k} \cdot \left(1 - SZk \right)}{\mathbf{K}_{virt} + \mathbf{c} + \mathbf{AG}_{virt} + \mathbf{W}_{virt} + \mathbf{AD}} \quad (28)$$

If there is disagreement then the physical properties of the materials should be checked, as should the measured data, in particular the moisture contents of the aggregates and the air content ($w_{AG,j}$ and *l*), and the calculations should be performed again using the corrected data. If it is not practicable to repeatedly measure the air content then *l* can be *calculated* using equations (18), (19) and (27). The calculated concrete composition content indicators may only be regarded as acceptable if the calculated density and water content do not deviate by more than 3% from the measured values, and if they are also consistent with the measured values.

Table 3 presents a possible example of how the dosage quantities and physical properties of the concrete constituents can be collected and recorded systematically for a particular batch of concrete. In the white fields at the bottom of the table we have highlighted the content indicators as calculated from the equations introduced, which clearly define the structural composition of the concrete in accordance with the basic model presented.

Components of concrete		Weight of coponents for the batch			Ratios in components		Fines (particles smaller than 0.063 mm)		Dried densities		Moisture content		Absorption of water	
marking	name	[kg/m^3]		[m^3/m^3]	marking	value	marking	[m%]	marking	[kg/m^3]	marking	[m%]	marking	[m%]
W_{virt}	*drilled water*	*285*							ρ_w =	*999*				
AD	*water reducing admixture*	*7,00*			$\alpha_{M,AD,1}$ =	*1,000*			$\rho_{AD,1}$ =	*1230*	*1-sz* $_1$ =	*61,0%*		
c	*CEM I 42,5 N*	*693*							ρ_c =	*3076*			sw_c =	*1,35%*
K_{virt}	*limestone filler*	*250*			$\alpha_{M,Kvirt,1}$ =	*1,000*	$\phi_{K,1}$ =	*80,0%*	$\rho_{K,1}$ =	*2699*			$sw_{K,1}$ =	*0,50%*
AG_{virt}	*0/4* $_{virt}$	*6072*	*2278*		$\alpha_{M,AGvirt,1}$ =	*0,375*	$\phi_{AG,1}$ =	*0,4%*	$\rho_{AG,fine,1}$ =	*2550*	$w_{AG,1}$ =	*4,4%*	$sw_{AG,1}$ =	*0,19%*
									$\rho_{AG,coarse,1}$ =	*2609*				
	4/8 $_{virt}$		*1279*		$\alpha_{M,AGvirt,2}$ =	*0,211*	$\phi_{AGvirt,2}$ =	*0,3%*	$\rho_{AG,fine,2}$ =	*2550*	$w_{AG,2}$ =	*3,3%*	$sw_{AG,2}$ =	*0,96%*
									$\rho_{AG,coarse,2}$ =	*2640*				
	8/16 $_{virt}$		*1158*		$\alpha_{M,AGvirt,3}$ =	*0,191*	$\phi_{AGvirt,3}$ =	*0,2%*	$\rho_{AG,fine,3}$ =	*2550*	$w_{AG,3}$ =	*2,2%*	$sw_{AG,3}$ =	*1,01%*
									$\rho_{AG,coarse,3}$ =	*2618*				
	16/32 $_{virt}$		*1357*		$\alpha_{M,AGvirt,4}$ =	*0,223*	$\phi_{AGvirt,4}$ =	*0,2%*	$\rho_{AG,fine,4}$ =	*2550*	$w_{AG,4}$ =	*1,3%*	$sw_{AG,4}$ =	*0,95%*
									$\rho_{AG,coarse,4}$ =	*2620*				
l	*air (void)-content (measured)*			*0,022*										
calculated concrete composition content indicators:		$V_{concrete}$= **3,054**		m^3	*p*= **0,238**		*x*= **1,356**		λ_{AD}= **0,019**		χ_c= **0,736**		v/c= **0,62**	
		$\rho_{concrete}$= **2392**		kg/m^3	w_{beton}= **6,41%**									

Table 3. Raw data from a specific batch of concrete, and the concrete composition content indicators calculated using equations (13) to (22) (evaporation was not accounted for here, ΔW_{ev}=0).
3. táblázat Egy konkrét betonszállítmány alapadatai és a (18) – (26) képletekből számított betonösszetételi állapotjelzői (párolgással nem számoltunk, ΔW_{ev}=0)

9. Data from the observations made at the mixing plant: experiences and conclusions

We began to collect and analyse the data from measurements and observations at the mixing plant in 2008. The data constituted the basic input for the data processing. At the end of the first year an interim evaluation was carried out. Observation data for compressive strength in 114 cases and for consistency in 119 cases were evaluated. The ranges of the concrete composition content indicators from the first year are shown in *Table 4*, while the structural compositions of the batches of concrete are presented graphically in *Fig. 2*.

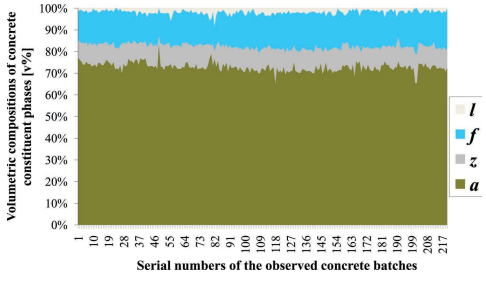

Fig. 2. Volumetric compositions of concrete constituent phases during observations
2. ábra A betonalkotó fázisok térfogatos összetételei a megfigyelések során

In the first period between 2008 and 2009, we were able to analyse the effects of several *types of cement* and several *water-reducing agents* in the case of concrete compositions with different *p* paste ratio and *x* fluid-paste powder volume ratios. With regard to the effect imposed on concrete compressive strength by the type of cement used, beyond the traditionally accepted influence (i.e. *water-cement ratio* is closely related to the compressive strength), we also found that the *cement dosage* ratio is a factor of at least of equal importance, and when we take the *two factors together*, the estimation of the compressive strength has a high degree of accuracy, in the case of mixes with identical air contents in the observed *p-x* ranges. We also found that the effect imposed on compressive strength by the *x* fluid-powder volume ratio is very similar to that of w/c.

	p	x	χ_c	λ_{AD}*	l
min	0,159	1,140	0,562	0,000	0,000
max	0,327	3,874	1,000	0,031	0,076
average	0,265	1,828	0,856	0,012	0,007
st. dev	0,02	0,33	0,09	0,01	0,01

Table 4. Concrete composition content indicators from the first period of manufacturing plant observations
4. táblázat A betonösszetételi állapotjelzők alakulása a gyártóüzemi megfigyelések első szakaszában

For illustration purposes, *Figs. 3* to *6* show the compressive strength relations observed. It can be seen at the identically scaled figures that the approximation functions inserted beside the measured compressive strength values do not run in parallel with the presented CEM I 42.5 and CEM III/A 32.5 cements, which is of course no surprise, but there is one important conclusion to be drawn, which has already been stated by *Ujhelyi* [7] in his findings on the water sensitivity of cements, and which is summarised *Kausay* in his comprehensive essay on the water-cement ratio [11] as: "By the water sensitivity of cements *Ujhelyi* means that different types of cement behave in different ways when the dosage of water is different (and therefore the water-cement ratio is different), for example, there are certain cements whose compressive strength decreases more rapidly than that of other cements as the dosage of water increases, and vice versa." In other words, cements cannot be typified in absolute figures (such as nominal compressive strength) but only *with their particular characteristics*, which in turn – as we can add with reference to our own observations – depend on the concrete composition content indicators. It is not only the effect of cements, however, that can be described *with characteristics*, but also the effect of *water-reducing agents*.

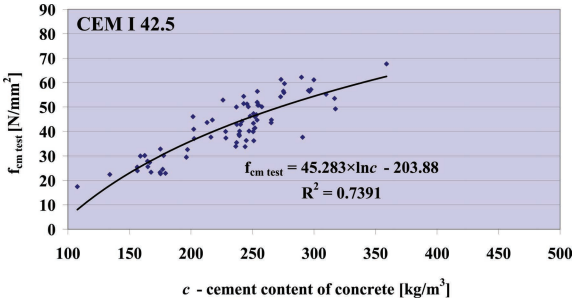

Fig. 3. The relationship between compressive strength and quantity of CEM I 42.5, based on observation data taken between 2008–2009
3. ábra A szilárdság függése a CEM I 42,5 mennyiségétől a 2008–2009 közötti megfigyelési időszak adatai szerint

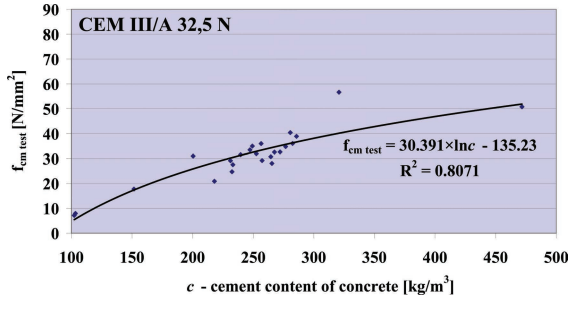

Fig. 4. The relationship between compressive strength and quantity of CEM III/A 32.5, based on observation data taken between 2008–2009
4. ábra A szilárdság függése a CEM III/A 32,5 mennyiségétől a 2008–2009 közötti megfigyelési időszak adatai szerint

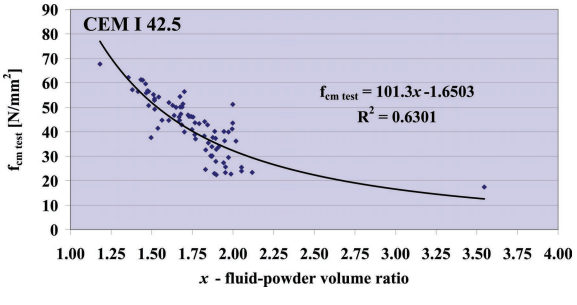

Fig. 5. Relationship between compressive strength and the x fluid-powder volume ratio for CEM I 42.5, based on observation data taken between 2008–2009
5. ábra A szilárdság függése CEM I 42,5 esetében az x folyadék-por térfogati tényezőtől a 2008–2009 közötti megfigyelési időszak adatai szerint

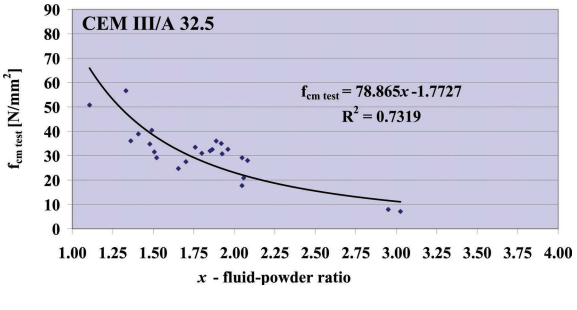

Fig. 6. Relationship between compressive strength and the x fluid-powder volume ratio for CEM III/A 32.5, based on observation data taken between 2008–2009
6. ábra A szilárdság függése CEM III/A esetében az x folyadék-por térfogati tényezőtől a 2008–2009 közötti megfigyelési időszak adatai szerint

Space limitation of present paper let us illustrate only on a few diagrams the widely differing effects experienced with certain water-reducing agents – compared both to each other and with concrete compositions without agents (*Figs. 7* to *10*).

It is indeed true that the water-reducing capacity of the agents depends on the concrete composition content indicators, so in these instances it is not enough to simply carry out the essential *single-factor* impact assessment (generally restricted to w/c = 0.5) that is suggested in the harmonised EN product standards.

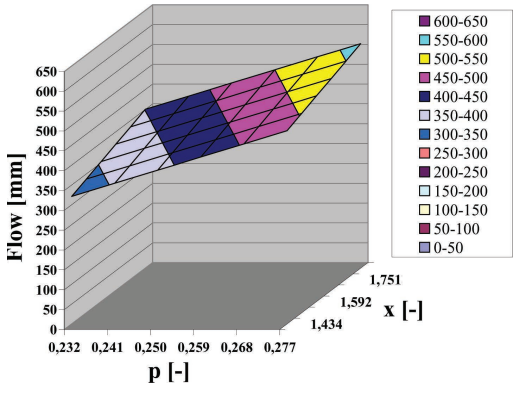

Fig. 7. The effect of a normal range water-reducing agent (λ_{AD} = 1.05% v/v) on the flow of fresh concrete
7. ábra Erős vízcsökkentő (λ_{AD} = 1,05% v/v) adalékszer hatása a betonkeverékek terüléseire

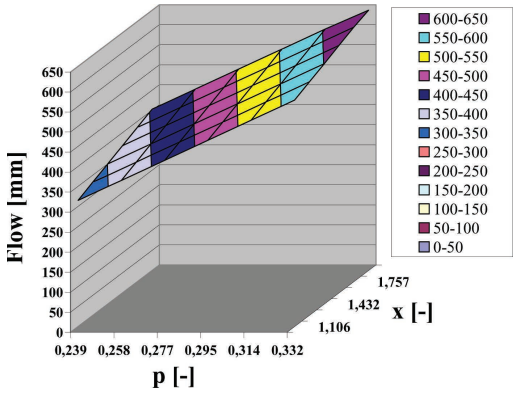

Fig. 8. The effect of a high range water-reducing agent (λ_{AD} = 1.23% v/v) on the flow of fresh concrete
8. ábra Kiváló vízcsökkentő (λ_{AD} = 1,23% v/v) adalékszer hatása a betonkeverékek terüléseire

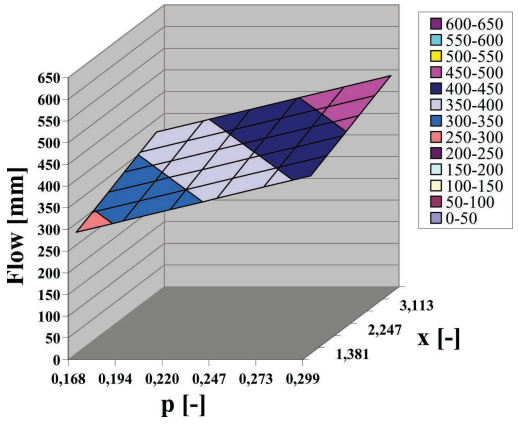

Fig. 9. Consistencies without water-reducing agents in the case of maximum size of aggregate D_{max} = 24 mm
9. ábra Vízcsökkentő adalékszer nélküli konzisztenciák 24 mm legnagyobb szemnagyságú adalékanyagok esetén

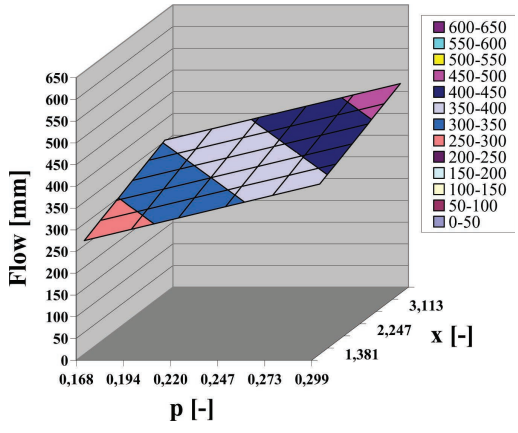

Fig. 10. Consistencies without water-reducing agents in the case of maximum size of aggregate D_{max} = 16 mm
10. ábra Vízcsökkentő adalékszer nélküli konzisztenciák 16 mm legnagyobb szemnagyságú adalékanyagok esetén

Acknowledgements

The author wishes to express his gratitude to the Augusztin Betongyártó Ltd. concrete mixing plant and particularly to Mr. Bálint Augusztin, CEO.

References

[1] Szalai K. – Huszár Zs. – Spránitz F.: *Betonszerkezeti EU szabványok hazai bevezetése, alkalmazása, 6. fejezet: HSC/HPC betonok és hídépítési alkalmazása.* Magyar Betonszövetség, Magyar Betonelemgyártó Szövetség, Magyar Építőanyagipari Szövetség, Budapest, 2005.
[2] Zsigovics, I.: *Self Compacting Concrete, Newest Revolution of Concrete Technology 3. Influence of limestone powder on the properties of fresh and hardened concrete.* Vasbetonépítés, 2004/3, pp. 72-79.
[3] Sulyok, T.: *Metróállomások építése az Etele téren és a körtéren.* Beton, XIV. évf. 10. szám, 2006. október, pp 26-27.
[4] Sulyok, T.: *Beszámoló az M6 autópályán épülő alagutakról – betontechnológus szemmel.* Beton, XVII. évf. 5. szám, 2009. május, pp 10-13.
[5] Spránitz, F.: *Érdemes-e küszködni az NT betonokkal? 4. rész – avagy milyen neműek a nagy teljesítőképességű (NT) betonok?* Beton, XVII. évf. 1. szám, 2009. január, pp 3-7.
[6] Powers, T. C. 1900-1997: Bibliography, PCA Library Bibliography No.33 (LB33), Portland Cement Association, 2007
[7] Ujhelyi, J.: *Betonismeretek.* Műegyetemi Kiadó. Budapest, 2005.
[8] *MÉASZ ME-04.19:1995 Műszaki előírás beton és vasbeton készítésére.* Magyar Építőanyagipari Szövetség, Budapest, 1995.
[9] Spránitz, F.: *Magas- és mélyépítési termékek újszerű gyártástechnológiái.* Beton, XVI. évf. 2. szám, 2008. február, pp 14-16.
[10] Powers, T. C.: *Absorption of Water by Portland Cement Paste during the Hardening Process.* Industrial and Engineering Chemistry, July 1935, Vol. 27, No. 7, pp 790-794.
[11] Kausay, T.: *Víz-cement tényező, víz/cement tényező.* Beton, XVI. évf. 4. szám, 2008. április, pp 8-11.

Ref.:
Gyula **Pekár**: *Simple basic model for concrete and its application. 1. Content indicators of concrete mixtures and mixing plant observations*
Építőanyag, 65. évf. 2. szám (2013), 52–60. p.
http://dx.doi.org/10.14382/epitoanyag-jsbcm.2013.12

Betonkeverékek egyszerűsített alapmodellje és alkalmazása.
1. rész: Betonösszetételi állapotjelzők és gyártóüzemi megfigyelések

A betontechnológia állandó feladata a betonalkotó anyagok hatásainak vizsgálata. E hatások elemzése és a tapasztalt összefüggések értelmezése során időről időre érdemes átgondolni azokat a modelleket, amelyekben a tapasztalt hatásokat értelmezzük. Ha szükséges, akkor finomításokkal is kell élnünk, hogy az új anyagok megjelenésével a betontervezés alapjául szolgáló modellek is lépést tarthassanak. A cikk a betonkeverékek összetételének egy leegyszerűsített alapmodelljét mutatja be, bevezetve a betonösszetételt egyértelműen meghatározó, dimenzió nélküli állapotjelzőket, amelyekről feltételezhető, hogy a betonok teljesítményjellemzőit befolyásolják, így vizsgálatuk szükségszerű. A modell kidolgozását egy gyártóüzemi megfigyelési sorozat indította el. Ez a gyártóüzemi megfigyelés szolgált az első alapadat-forrásként a betonkeverékek egyszerűsített alapmodelljéhez, amely a dimenzió nélküli beton összetételi állapotjelzők bevezetésével újszerű lehetőségeket kínál a friss és megszilárdult betonkeverékek teljesítményjellemzőit befolyásoló hatások vizsgálatára.
Kulcsszavak: betontechnológia, betonösszetétel tervezése, betonösszetételi állapotjelzők

TRANSCEND CONFERENCE
Water Transport in Cementitious Materials

November 3–6, 2013, Guildford, UK
http://www.nanocem.org/TRANSCEND-MC-ITN

Venue:
The conference will be held at the conference center, Radisson Blu Edwardian Guildford Hotel in Guildford, UK.

TRANSCEND Research themes and projects:

Modelling – The theme comprises five projects that systematically build a theoretical understanding of water dynamics in cements and concretes at a hierarchy of length scales: Molecular dynamics study of water exchange between inter-sheet and gel pore in cement analogues; Moisture transport in random media: Calcium Silicate Hydrate (C-S-H); Lattice Boltzmann modeling of water dynamics in cement paste; The role of microcracks in concrete on water transport; Drying-wetting cycles: effects on moisture transport within cementitious materials.
Experimental – The theme comprises six projects that build the experimental parameter database such as characterisation of materials and transport coefficients needed as input to the modelling developed in Theme Modelling: Wetting and drying cycles: effects of hysteresis on transport; Study of white cement pastes by nuclear magnetic resonance (NMR); Relationship between composition, structure and morphology in C-S-H; nuclear magnetic resonance imaging and relaxation analysis of cement based material; Cryoporometry characterisation for cement based materials; Characterisation of microcracks in concrete and transport in concrete.
Validation – The theme comprises four projects that together validate the output at the different length scales of the modelling programme: Transport and water dynamics in the nanopores of C-S-H; Impact of mineralogy on the water balance of cement paste; Validation of concrete water transport tests by 1H magnetic resonance profiling; Validation of modeling with respect to drying and shrinkage.

GUIDELINE FOR AUTHORS

The manuscript must contain the followings: title; author's name, workplace, e-mail address; abstract, keywords; main text; acknowledgement (optional)**; references; figures, photos with notes; tables with notes; short biography** (information on the scientific works of the authors).

The full manuscript should not be more than 6 pages including figures, photos and tables. Settings of the word document are: 3 cm margin up and down, 2,5 cm margin left and right. Paper size: A4. Letter size 10 pt, type: Times New Roman. Lines: simple, justified.

TITLE, AUTHOR

The title of the article should be short and objective.
Under the title the name of the author(s), workplace, e-mail address.
If the text originally was a presentation or poster at a conference, it should be marked.

ABSTRACT, KEYWORDS

The abstract is a short summary of the manuscript, about a half page size. The author should give keywords to the text, which are the most important elements of the article.

MAIN TEXT

Contains: materials and experimental procedure (or something similar), results and discussion (or something similar), conclusions.

REFERENCES

References are marked with numbers, e.g. [6], and a bibliography is made by the reference's order.
Examples:
Journals:
[6] K. R. Mohamed – Z. M. El-Rashidy – A. A. Salama: *vitro properties of nano-hydroxyapatite/chitosan biocomposites.* Ceramics International. **37**(8), December 2011, pp. 3265–3271, http://dx.doi.org/10.1016/j.ceramint.2011.05.121
Books:
[6] C. Barry Carter – M. Grant Norton: *Ceramic Materials Science and Engineering*. Springer Science + Business Media, LLC; New York, 2007.

FIGURES, TABLES

All drawings, diagrams and photos are figures. The **text should contain references to all figures and tables**. This shows the place of the figure in the text. Please send all the figures in attached files, and not as a part of the text. **All figures and tables should have a title**.
Authors are asked to submit color figures by submission. Black and white figures are suggested to be avoided, however, acceptable.
The figures should be: tiff, jpg or eps files, 300 dpi at least, photos are 600 dpi at least.

BIOGRAPHY

Max. 500 character size professional biography of the author(s).

CHECKING

The editing board checks the articles and informs the authors about suggested modifications. Since the author is responsible for the content of the article, the author is not liable to accept them.

CONTACT

Please send the manuscript in electronic format to the following e-mail address: femgomze@uni-miskolc.hu and epitoanyag@szte.org.hu or by post: Scientific Society of the Silicate Industry, Budapest, Bécsi út 122–124., H-1034, HUNGARY

We kindly ask the authors to give their e-mail address and phone number on behalf of the quick conciliation.

INHALT

СОДЕРЖАНИЕ

European Commission

CORDIS

Community Research and Development Information Service

endure – European Network for Durable Reinforcement and Rehabilitation Solutions

Marie Curie Actions— Initial Training Networks (ITN)

FP7-PEOPLE-2013-ITN

The growth of advanced composites in construction in recent years has been spectacular, doubling in size in the last 10 years. This expansion has been largely due to the use of Fibre Reinforced Polymer (FRP) reinforcement in structural applications and, although the current economic climate has seen a slowdown of the general construction market, the demand of composite products within the European construction market is estimated to grow and reach €3.1 billion by 2013.

The on-going requirement for more durable structures and more efficient rehabilitation solutions is the key driving force behind the introduction of FRPs in the construction industry as reinforcing or strengthening material for concrete and masonry structures. In Europe alone, the annual cost of repair and maintenance of the infrastructure is estimated to be about 50% of the construction budget.

Composite materials are readily used in a large number of applications and yet, a set of accepted design guidelines does not exist and most construction professionals are unaware of what composites are and rely on specialists who often use their own standards and guidelines.

Moreover, little interaction exists between academia and industry and practical applications are time and again a reflection of a design approach instructed by conservative guidelines, which hinder innovation.

The aim of the Network is to train researchers in the use of advanced composites for construction so as to develop and maintain a critical mass of research groups that will address the main scientific challenges in the field, enable the development of advanced material standards and design guidelines, co-ordinate European research, and offer a link between academia and industry.

The Network aims:

- To address the specific scientific/technological challenges in the field and develop tests, models and advanced guidelines to help with the standardisation process.
- To bridge the gap between academia and industry and increase the competitiveness of the European composite and construction industry worldwide.

The Network will strengthen the European Research Area on composite reinforcements and will contribute to increase the competitiveness of the European construction industry worldwide.

The key objective of the endure network is training and career development of young researchers. The Network will provide early stage and experienced researchers with advanced training in research methods as well as transferable skills. Researchers will undertake, as part of their research projects, secondments and study visits to other network partners and Associated Partners. These exchange visits will enable researchers to take advantage of internationally-leading expertise within the network, develop their own networks, and promote collaboration and discussion across the network. The interaction with the Associated Partners and representatives from the Industry during the planned network events will also give researchers an all-round education to prepare them equally for employment in industry or academia.

Network participants:

The University of Sheffield (USFD), UK (person in charge of scientific aspects of the Network: Dr. Maurizio Guadagnini); *Budapesti Műszaki és Gazdaságtudományi Egyetem* (BME), HU; *Universiteit Gent* (UGent), NL; *University of Bath* (UBAH), UK; *Universita degli Studi di Padova* (UNIPD), IT; *Politecnico di Milano* (POLIMI), IT; *Latvijas Universitates Polimeru Mehanikas Instituts* (LUPMI), LV; *Universidade do Minho* (UMINHO), PT; *Lulea Tekniska Universitet* (LTU), SE; *Universitat De Girona* (UdG), ES; *Eidgenoessische Materialpruefungs- und Forschungsanstalt* (EMPA), CH; *Netcomposites Limited* (NetComp), UK; *University of Patras* (UPAT), GR; *Technische Universitaet Kaiserslautern* (UNIKL), DE.

For further information refer to the website of the **endure** Network:

http://cordis.europa.eu/projects/rcn/109364_en.html

SEVENTH FRAMEWORK PROGRAMME

Marie Curie Actions - Initial Training Networks (ITN) of the Seventh Framework Programme (FP7) are supported by the European Union

CORDIS Community Research and Development Information Service is managed by the Publications Office of the European Union